arXiv:2601.11471v1 [cs.LG] 16 Jan 2026

Low-Rank Key Value Attention

James O'Neill[†] **Robert Clancy** **Mariia Matskevichus** **Fergal Reid**
AI Group, Intercom
124 St Stephen's Green, Dublin 2, D02 C628, Ireland
{james.oneill, rob.clancy, mariia.matskevichus, fergal.reid}@intercom.io

Abstract

Transformer pretraining is increasingly constrained by memory and compute requirements, with the key–value (KV) cache emerging as a dominant bottleneck during training and autoregressive decoding. We propose *low-rank KV adaptation* (LRKV), a simple modification of multi-head attention that reduces KV cache memory by exploiting redundancy across attention heads while preserving full token-level resolution. Each layer uses a shared full-rank KV projection augmented with low-rank, head-specific residuals, yielding a continuous trade-off between complete sharing and fully independent attention.

LRKV is a drop-in replacement for standard multi-head attention and directly subsumes query-sharing approaches such as multi-query and grouped-query attention, while remaining distinct from latent-compression methods such as multi-latent attention (MLA). Across large-scale pretraining experiments, LRKV consistently achieves faster loss reduction, lower validation perplexity, and stronger downstream task performance than standard attention, MQA/GQA, and MLA. At the 2.5B scale, LRKV outperforms standard attention while using roughly half the KV cache, and reaches equivalent model quality with up to **20–25% less training compute** when measured in cumulative FLOPs. To explain these gains, we analyze attention head structure in operator space and show that LRKV preserves nearly all functional head diversity relative to standard attention, whereas more aggressive KV-sharing mechanisms rely on compensatory query specialization. Together, these results establish LRKV as a practical and effective attention mechanism for scaling Transformer pretraining under memory- and compute-constrained regimes.

1 Introduction

Transformers are the dominant architecture for large-scale sequence modeling in language, vision, and multimodal domains (Vaswani et al., 2017; OpenAI, 2023), but as their size, sequence length, and context window grow, so does, rapidly, their computational and memory costs. KV-caching, which stores the atttention key and value representations, is a primary contributor to this overhead, as it spans every attention layer, and scales linearly with sequence length and count of heads. The cumulative KV footprint of modern models with tens of billion parameters can exceed the parameter memory itself, especially for long-context inference (Dao et al., 2024; Child et al., 2019).

A range of approaches have been proposed to alleviate the growing KV cache cost. Multi-Query Attention (MQA) (Shazeer, 2019) and Grouped-Query Attention (GQA) (Ainslie et al., 2023) reduce memory and latency by sharing key-value (KV) projections across heads or groups of heads, and are now standard in large-scale models such as PaLM and LLaMA (Touvron et al., 2023; 2024). However, aggressive KV sharing introduces a fundamental trade-off: while memory is reduced, head-level representational diversity is constrained, even though distinct attention heads are known to encode complementary syntactic and semantic patterns (Clark et al., 2019; Michel et al., 2019).

At the same time, empirical studies and recent spectral analyses show that attention heads are not fully independent: head-specific KV projections are highly correlated and occupy overlapping subspaces, indicating substantial redundancy (Yunis et al., 2024). Crucially, this redundancy is structured rather than uniform—small, head-specific variations remain important for capturing nuanced dependencies. This raises a natural question: *can KV memory be reduced by exploiting redundancy across heads, without collapsing the specialization that makes multi-head attention effective?*

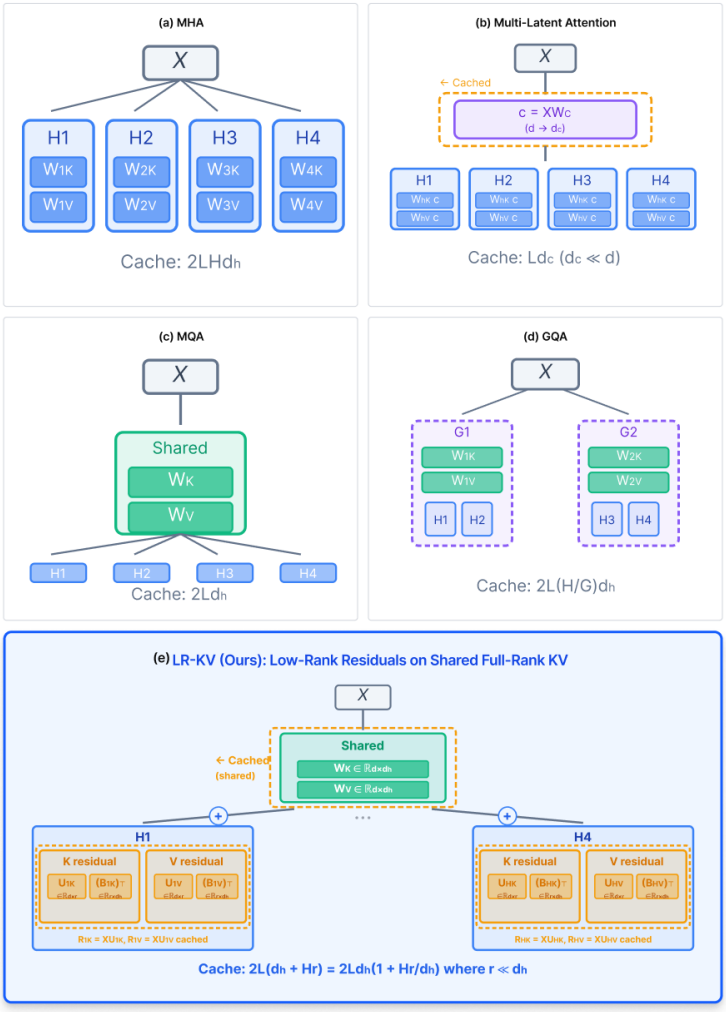

Figure 1: **Comparison of attention mechanisms and their KV cache costs.** (a) Multi-Head Attention (MHA) uses independent K/V projections per head with cache cost $2LHd_h$. (b) Multi-Latent Attention compresses inputs to latent dimension d_c before per-head projections (cache: Ld_c where $d_c \ll d$). (c) Multi-Query Attention (MQA) shares a single K/V across all heads (cache: $2Ld_h$) but suffers from low diversity. (d) Grouped-Query Attention (GQA) shares K/V within groups of heads (cache: $2L(H/G)d_h$), balancing efficiency and diversity. (e) Our proposed LR-KV method maintains shared full-rank W_K, W_V projections while each head adds a low-rank residual $U_h(B_h)^\top$ (rank $r \ll d_h$). We cache both the shared features and per-head latents $R_h = XU_h$, achieving cache cost $2L(d_h + Hr)$. Dashed boxes indicate cached components. LR-KV provides head diversity while maintaining cache efficiency comparable to MLA.

Beyond KV sharing, efficiency research has pursued complementary directions such as sparse or kernelized attention(Wang et al., 2020; Beltagy et al., 2020; Child et al., 2019), architectural optimizations(Dao et al., 2024) , and latent compression methods including Multi-Latent Attention (MLA)(Liu et al., 2024a). However, none of these approaches explicitly resolve the duplication of per-head key and value representations that dominates the KV memory footprint in large models.

In this work, we propose **Low-Rank KV Adaptation (LRKV)**, a simple and effective modification of multi-head attention that directly addresses this tension by exploiting structured redundancy across heads while preserving head specialization. Each Transformer layer maintains a single shared, full-rank key and value projection serving as a global basis across heads, while each head learns a

compact, trainable low-rank residual that perturbs the shared representations. The shared component encodes global relational structure, and the low-rank residuals restore the localized specialization that independent heads would otherwise provide. This factorization significantly reduces KV memory while retaining the head-level diversity critical for expressivity.

Unlike prior KV-sharing mechanisms, LRKV preserves a full-rank shared base to maintain representational capacity and learns per-head residuals jointly during pretraining. This provides a continuous spectrum between complete sharing (as in MQA) and full independence (as in standard attention), controlled by the residual rank parameter. Our experiments demonstrate that LRKV achieves 40–50% reductions in KV cache size with negligible impact on convergence, perplexity, or downstream performance. By aligning Transformer attention with its underlying spectral and informational structure, LRKV provides a practical foundation for scaling pretraining under memory-constrained regimes.

The design of LRKV differs from previous KV-sharing methods in two respects. First, it retains a full-rank shared component rather than constraining all heads to use the same low-rank representation, which maintains capacity for representing high-dimensional dependencies. Second, the low-rank residuals are trained jointly with the shared projection during pretraining, allowing the model to learn how much variation each head requires. This formulation provides a continuous trade-off between the efficiency of shared KVs and the flexibility of independent projections.

We evaluate LRKV on large-scale language model pretraining and downstream tasks, measuring validation loss, compute-normalized convergence, and KV cache usage across standard MHA, MQA/GQA, and MLA baselines. LRKV consistently improves loss reduction and downstream performance at a given compute budget while reducing KV cache memory by 40-50$\%$. We further provide an operator-space analysis of head diversity showing that LRKV preserves functional head specialization under compression, and characterize the role of residual rank in this trade-off. These findings establish that LRKV's empirical success stems from aligning with the natural low-rank structure of attention projections while preserving the degrees of freedom necessary for head specialization.

We evaluate LRKV on large-scale language modeling benchmarks and analyze its effect on pretraining dynamics, memory efficiency, and downstream generalization. Across model sizes, LRKV attains comparable perplexity and downstream accuracy to standard MHA while reducing KV cache size by a factor of two to four, depending on configuration. These results suggest that a large portion of per-head variation in KV representations can be captured through low-rank structure, and that explicit factorization offers a principled route to improving the memory efficiency of pretraining.

2 Related Work

The memory footprint of the key-value (KV) cache has become a central bottleneck in deploying large autoregressive Transformers. While early work improved the *computational* efficiency of attention via sparsity, kernelization, or low-rank approximations of the attention matrix (Child et al., 2019; Beltagy et al., 2020; Wang et al., 2020; Katharopoulos et al., 2020; Choromanski et al., 2021), these methods do not reduce KV-cache size and therefore provide limited benefit for decoding-heavy LLMs where memory, rather than compute, dominates inference cost.

Sharing K/V Projections. A widely adopted strategy for reducing KV memory is to share key and value projections across attention heads. Multi-Query Attention (MQA) (Shazeer, 2019) uses a single shared set of K/V projections, and Grouped-Query Attention (GQA) (Ainslie et al., 2023) extends this by sharing within small head groups. These approaches achieve substantial memory savings but sacrifice head-level expressivity. Analyses of pretrained models (Clark et al., 2019; Michel et al., 2019) consistently show that attention heads specialize for different syntactic or semantic functions; collapsing their projections can therefore degrade modeling quality. LRKV is motivated by this tension: we preserve the efficiency of shared projections while reintroducing diversity through low-rank head-specific residuals.

Low-Rank Parameterization of Attention Weights. Our formulation is related to low-rank reparameterization techniques such as LoRA (Hu et al., 2022), which add low-rank updates to weight matrices for parameter-efficient fine-tuning. Follow-up work extends this idea to training-time regularization or improved factorization schemes (Peng et al., 2025). However, these methods intervene on the *optimization pathway*, not on the structure of stored activations. LRKV applies the same

low-rank principle directly to attention projections, introducing low-rank *representational* deviations that shape the K/V features encoded in the cache.

Recent work has also explored low-rank or factored $Q/K/V$ projections to improve parameter efficiency or computational throughput (Xie et al., 2023; Khalaf et al., 2025). The concurrent work of Lv et al. (2024) investigates low-rank parameterizations of attention projections more broadly. These methods typically replace full-rank projections with low-rank ones to reduce computation. LRKV differs conceptually: we preserve a full-rank shared projection and add only low-rank head-specific residuals, enabling memory reduction while maintaining full-rank representational capacity.

KV-Cache Compression and Long-Context Modeling. A complementary body of research aims to compress or restructure the KV cache itself. Approaches include clustering or distilling K/V states (Chari et al., 2025), exact hybrid and compressed buffers (Yao et al., 2025; Li et al., 2024), token selection or pooling (Ge et al., 2023), and architectural changes that replace attention with recurrent or state-space alternatives (Sun et al., 2024). Unlike these activation-level methods, LRKV reduces the amount of information that must be stored by changing how each head generates its K/V features. Our hybrid long-context cache builds on this: exact short-range KVs are retained, while long-range information is reconstructed efficiently via low-rank residuals.

Comparison to Multi-Latent Attention. Multi-Latent Attention (MLA) (Liu et al., 2024a) reduces KV cache memory by compressing token representations into a shared low-dimensional latent space before caching. During attention, interaction with the cache therefore requires projecting queries and/or values through this latent bottleneck. This achieves strong memory compression but constrains all heads to operate through the same latent representation, limiting per-head expressivity and restricting positional encoding choices (e.g., requiring partial RoPE).

LRKV addresses a different source of redundancy. Rather than compressing information across tokens, LRKV preserves full token-level resolution and reduces redundancy *across heads* by factorizing each head's KV projection into a shared full-rank base plus low-rank head-specific residuals. This additive structure retains the original feature dimensionality, supports arbitrary positional encodings, and preserves head specialization while substantially reducing KV memory. As a result, LRKV and MLA represent complementary approaches: MLA compresses token space via a shared latent bottleneck, whereas LRKV compresses head space via structured sharing.

Factorized or Shared KV Mechanisms. Concurrent work explores structured KV-cache reduction via factorized representations (e.g., MFA/MFA-KR; TPA (Hu et al., 2025; Zhang et al., 2025)) explores structured compression across heads. LRKV provides a principled middle ground between fully shared (MQA/GQA) and fully independent projections: the full-rank shared base captures global structure, while low-rank residuals preserve head-level variability. This structured additive decomposition is key for achieving memory savings without collapsing representational diversity.

Analyzing attention head diversity. Prior work has measured head redundancy using attention pattern similarity (Michel et al., 2019; Voita et al., 2019), activation-based metrics such as CKA (Kornblith et al., 2019), or SVCCA (Raghu et al., 2017). Recent work explicitly characterizes gauge symmetries in attention parameterizations (Wang & Wang, 2025), recognizing that per-head rotations preserve attention function. However, these approaches either compare raw weights (not gauge-invariant) or analyze activation space rather than the functional operators $\mathbf{W}^Q(\mathbf{W}^K)^\top$ that determine attention. We introduce a principled method combining gauge-invariant bilinear forms with centered Gram matrix analysis (kernel PCA) to measure intrinsic head diversity independent of parameterization choices.

3 Methodology

Transformers represent each token in a sequence through queries, keys, and values that interact via scaled dot-product attention. For an input matrix $\mathbf{X} \in \mathbb{R}^{L\times d}$, the h-th attention head computes

$$\mathbf{Q}_h = \mathbf{X}\mathbf{W}_h^Q, \qquad \mathbf{K}_h = \mathbf{X}\mathbf{W}_h^K, \qquad \mathbf{V}_h = \mathbf{X}\mathbf{W}_h^V,$$

where $\mathbf{W}_h^{Q,K,V} \in \mathbb{R}^{d\times d_h}$ and $d_h = d/H$ for H heads. The head output is

$$\mathbf{O}_h = \mathrm{softmax}\left(\frac{\mathbf{Q}_h\mathbf{K}_h^\top}{\sqrt{d_h}}\right)\mathbf{V}_h,$$

and outputs from all heads are concatenated and projected to form the layer output. During autoregressive decoding, the KV cache stores $\mathbf{K}_h$ and $\mathbf{V}_h$ for all previous tokens and heads, incurring per-layer memory

$$M_{\text{standard}} = 2LHd_h = 2Ld.$$

Motivation. Empirical studies show attention heads within a layer are often correlated (Clark et al., 2019; Michel et al., 2019), suggesting that per-head key/value features contain substantial redundancy. Existing KV-sharing methods such as MQA and GQA reduce cache size by sharing K/V across heads, but can reduce head diversity and modeling capacity. Our goal is to reduce redundant KV storage while preserving head-specific flexibility.

Low-Rank KV Adaptation (LRKV). We parameterize each head's key/value projection as a shared base plus a head-specific low-rank residual, while keeping the resulting projection shape $d \times d_h$:

$$\mathbf{W}_h^K = \mathbf{W}_{\text{shared}}^K + \mathbf{U}_h^K \mathbf{B}_h^{K\top}, \qquad \mathbf{W}_h^V = \mathbf{W}_{\text{shared}}^V + \mathbf{U}_h^V \mathbf{B}_h^{V\top}, \tag{1}$$

where

$$\mathbf{W}_{\text{shared}}^{K,V} \in \mathbb{R}^{d\times d_h}, \quad \mathbf{U}_h^{K,V} \in \mathbb{R}^{d\times r}, \quad \mathbf{B}_h^{K,V} \in \mathbb{R}^{d_h\times r}, \quad r \ll d_h.$$

The effective keys and values are

$$\mathbf{K}_h = \mathbf{X}\mathbf{W}_h^K, \qquad \mathbf{V}_h = \mathbf{X}\mathbf{W}_h^V.$$

When $r = 0$, LRKV reduces to complete KV sharing (MQA-style) within a layer; increasing r interpolates toward standard MHA. All parameters in Equation 1 are optimized jointly during pretraining. Gradients from the shared and residual paths are additive, allowing the model to learn how much per-head variation is required. LRKV constrains head-specific projections to an affine family centered at $\mathbf{W}_{\text{shared}}^{K,V}$, providing a continuous spectrum between full sharing ($r = 0$) and full independence (large r).

LRKV caching scheme. During decoding, the bottleneck is storing $\mathbf{K}_h, \mathbf{V}_h \in \mathbb{R}^{L\times d_h}$ for every head. LRKV caches a shared component once per layer and compact per-head latents:

1. **Shared features (cached once per layer):**

$$\mathbf{K}_{\text{shared}} = \mathbf{X}\mathbf{W}_{\text{shared}}^K \in \mathbb{R}^{L\times d_h}, \qquad \mathbf{V}_{\text{shared}} = \mathbf{X}\mathbf{W}_{\text{shared}}^V \in \mathbb{R}^{L\times d_h}.$$

2. **Per-head low-rank latents (cached per head):**

$$\mathbf{R}_h^K = \mathbf{X}\mathbf{U}_h^K \in \mathbb{R}^{L\times r}, \qquad \mathbf{R}_h^V = \mathbf{X}\mathbf{U}_h^V \in \mathbb{R}^{L\times r}.$$

The full per-head features can be expressed as

$$\mathbf{K}_h = \mathbf{K}_{\text{shared}} + \mathbf{R}_h^K \mathbf{B}_h^{K\top}, \qquad \mathbf{V}_h = \mathbf{V}_{\text{shared}} + \mathbf{R}_h^V \mathbf{B}_h^{V\top}. \tag{2}$$

Attention computation without explicit reconstruction. Naively materializing $\mathbf{K}_h, \mathbf{V}_h$ for all cached tokens would cost $O(Lrd_h)$. Instead, we exploit associativity to avoid forming $\mathbf{K}_h, \mathbf{V}_h$ explicitly. For a decoding step with query $\mathbf{q}_h \in \mathbb{R}^{d_h}$,

$$\mathbf{q}_h \mathbf{K}_h^\top = \mathbf{q}_h \mathbf{K}_{\text{shared}}^\top + (\mathbf{q}_h \mathbf{B}_h^K)\,(\mathbf{R}_h^K)^\top, \tag{3}$$

and for attention weights $\mathbf{a}_h \in \mathbb{R}^{1\times L}$,

$$\mathbf{a}_h \mathbf{V}_h = \mathbf{a}_h \mathbf{V}_{\text{shared}} + (\mathbf{a}_h \mathbf{R}_h^V)\,\mathbf{B}_h^{V\top}. \tag{4}$$

Equation 3 and Equation 4 enable LRKV to be implemented inside fused attention kernels without reconstructing full per-head KV tensors.

To situate LRKV relative to existing attention mechanisms, Table 1 summarizes how different methods parameterize key/value projections and where compression is applied.

KV cache memory complexity (during decoding). Standard attention stores per-head keys and values:

$$M_{\text{standard}} = 2LHd_h.$$

Table 1: **Mathematical comparison of attention mechanisms.** We compare how different mechanisms parameterize key/value projections and where compression is applied. Here $X \in \mathbb{R}^{T\times d}$ is the token sequence, $d_h = d/H$ is the head dimension, H is the number of heads, and $r, d_c \ll d_h$.

Method	KV projection form	Rank constraint	Compression axis
Standard MHA	$W_h^{K,V} \in \mathbb{R}^{d\times d_h}$ (independent per head)	None (full rank)	None
MQA	$W_h^{K,V} = W_{\text{shared}}^{K,V}\ \forall h$	$\text{rank}(W_h^{K,V}) = \text{rank}(W_{\text{shared}})$	Across heads (complete sharing)
GQA	$W_h^{K,V} = W_{g(h)}^{K,V}$ for group $g(h)$	Full rank within group	Across heads (group-wise sharing)
MLA	$W_h^{K,V} = W_{\text{down}} W_{\text{up},h}^{K,V}$	$\text{rank}(W_h^{K,V}) \le d_c$	Across tokens (latent bottleneck)
LRKV (ours)	$W_h^{K,V} = W_{\text{shared}}^{K,V} + U_h^{K,V}(B_h^{K,V})^\top$	$\text{rank}(W_h^{K,V} - W_{\text{shared}}^{K,V}) \le r$	Across heads (additive low-rank deviations)

LRKV stores shared $\mathbf{K}_{\text{shared}}, \mathbf{V}_{\text{shared}}$ once per layer plus per-head latents:

$$M_{\text{LRKV}} = \underbrace{2Ld_h}_{\text{shared } (K,V)} + \underbrace{2LHr}_{\text{per-head latents } (R^K, R^V)} = 2L(d_h + Hr). \tag{5}$$

Thus the memory ratio is

$$\frac{M_{\text{LRKV}}}{M_{\text{standard}}} = \frac{d_h + Hr}{Hd_h} = \frac{1}{H} + \frac{r}{d_h}. \tag{6}$$

Compute overhead during decoding (FLOPs). Per decoding step, standard attention has dominant per-head computational cost $O(Ld_h)$ from query-key dot products and value aggregation. Using the distributed forms in Equation 3 and Equation 4, LRKV adds an extra

$$\Delta\text{FLOPs} = O(Lr + rd_h)$$

per head per decoding step.

Parameter complexity. Standard per-layer K/V parameters scale as $2Hdd_h$. LRKV uses a shared base plus low-rank factors:

$$P_{\text{LRKV}} = \underbrace{2dd_h}_{\text{shared } (K,V)} + \underbrace{2Hr(d + d_h)}_{\text{per-head low-rank factors}}, \tag{7}$$

which can be lower or higher than standard depending on (H, r, d_h); in practice we choose r to prioritize KV-cache reduction with minimal quality impact. In our experiments, LRKV remains competitive or better even when r is chosen so that the K/V parameter count is below standard MHA.

4 Shared Subspaces, Spectral Bias, and Information Structure

The MHA mechanism was originally introduced to allow multiple attention "views" of the same sequence, with different heads capturing complementary dependencies (Vaswani et al., 2017). However, empirical analysis of pretrained Transformers reveals that many attention heads are highly correlated and often attend to overlapping tokens or features (Clark et al., 2019; Michel et al., 2019; Bhojanapalli et al., 2021). This redundancy suggests that head-specific projections inhabit a shared, low-dimensional manifold shaped by statistical regularities in the data and by the optimization biases of gradient descent. **LRKV** can be viewed as an explicit parameterization of this structure, disentangling global and head-specific information within a single architectural formulation.

Shared subspace and spectral structure. Prior empirical analyses of pretrained Transformers have shown that attention heads exhibit substantial redundancy and occupy overlapping subspaces (Michel et al., 2019; Clark et al., 2019; Bhojanapalli et al., 2021; Rahaman et al., 2019). To assess

this structure in a gauge-invariant manner, we analyze attention bilinear forms $\mathbf{A}_h = \mathbf{W}_h^Q(\mathbf{W}_h^K)^\top$ and measure head diversity via PCA on their centered Gram matrix (subsection 6.3). We find that LRKV achieves 93.5% effective rank versus 94.0% for standard MHA at 2.5B scale, confirming that heads occupy nearly independent dimensions in bilinear form space despite using shared key-value bases. This validates that the functional behavior of attention projections lies near a shared low-dimensional manifold, with LRKV's additive structure explicitly parameterizing this geometry. Importantly, while heads remain functionally diverse, the *individual* weight matrices $\mathbf{W}_h^K$ exhibit low intrinsic rank—they concentrate energy in a small number of dominant singular directions.

Such spectral concentration is consistent with the *spectral bias* of neural networks (Rahaman et al., 2019; Fang & Xu, 2024), whereby gradient-based optimization preferentially amplifies smooth, high-variance modes before fitting higher-frequency residual structure. As a result, attention projections tend to concentrate energy in a small set of globally shared directions. LRKV makes this implicit organization explicit: the shared projections $\mathbf{W}_{\text{shared}}^{K,V}$ capture dominant spectral components, while per-head low-rank residuals model localized refinements aligned with lower-variance directions. Each head therefore operates within an affine subspace centered on $\mathbf{W}_{\text{shared}}^{K,V}$, with a tangent space spanned by a compact set of learned low-rank factors.

Residual rank as a control knob for diversity. In LRKV, the residual rank r controls a continuous spectrum between fully shared keys/values and fully independent per-head projections. At a high level, the shared base $\mathbf{W}_{\text{shared}}^{K,V}$ serves as a common coordinate system capturing features that are broadly useful across heads, while the low-rank residuals provide a budgeted mechanism for head specialization. When r is small, heads are strongly coupled through the shared representation; as r grows, the model can allocate additional degrees of freedom to capture head-specific patterns. This view motivates treating r as an architectural hyperparameter with a clear interpretation: it directly controls the efficiency-diversity trade-off in the KV cache and per-head specialization. Empirically, we find that $r \approx 0.5 \times d_h$ provides the critical threshold: LRKV achieves 93.5% PCA-based effective rank versus 94.0% for standard MHA at 2.5B scale (subsection 6.3), confirming that moderate rank suffices to preserve nearly all head diversity while achieving substantial cache reduction.

Decomposition geometry and (non-)orthogonality. The decomposition $\mathbf{W}_h = \mathbf{W}_{\text{shared}} + \mathbf{U}_h\mathbf{B}_h^\top$ is not identifiable: for any Δ, we can shift $\mathbf{W}_{\text{shared}} \leftarrow \mathbf{W}_{\text{shared}} + \Delta$ and $\mathbf{U}_h\mathbf{B}_h^\top \leftarrow \mathbf{U}_h\mathbf{B}_h^\top - \Delta$ without changing $\mathbf{W}_h$. In unconstrained Euclidean parameter space there is therefore no *a priori* reason to expect strict orthogonality between the shared and residual terms. Instead, we use overlap (e.g., cosine similarity or subspace angles) as a diagnostic: low overlap indicates that the residual contributes directions not already captured by the shared component, reducing redundant parameterization. In practice, any tendency toward reduced overlap is an emergent outcome of end-to-end training and the model's incentives to allocate capacity efficiently, rather than an explicit constraint or training objective.

Connection to low-rank approximation. LRKV can also be interpreted as learning a structured low-rank approximation of the family of per-head projections. In classical matrix approximation, the optimal rank-r representation is given by truncated SVD with respect to a chosen error metric. LRKV differs in two important ways: (i) it learns the shared and residual factors *jointly* with the rest of the network under the task loss, and (ii) the residual factors are head-specific, enabling specialization without requiring each head to store full-rank keys/values. This perspective suggests that end-to-end training can discover factorizations that are close to classical optima while remaining aligned with the functional requirements of attention.

Scaling, normalization, and stability. Because LRKV is additive, the norms of the shared and residual components can evolve independently during training. However, attention depends primarily on *directional* structure and relative alignment, and common transformer normalization (e.g., RMSNorm) reduces sensitivity to absolute scale. From this perspective, changes in parameter magnitudes are best interpreted as a redistribution of representational capacity between shared and residual pathways rather than as a direct indicator of instability. This motivates analyzing LRKV through geometry (alignment, overlap) and function (loss/perplexity), rather than through norms alone.

5 Experimental Setup

Pretraining Configuration. We pretrain from scratch a family of decoder-only Transformer language models with parameter counts of **128M** and **2.5B** on the **FineWeb-Edu** dataset. Unless otherwise stated, model scale (e.g., 128M, 2.5B) refers to the parameter count of the *base architecture with standard multi-head attention (MHA)*. Alternative attention mechanisms (LRKV, MQA, GQA, MLA) replace only the attention module while keeping all other architectural components fixed, which will result in reduced total parameter count due to reparameterized key-value projections.

For the large-scale runs (2.5B), we choose token budgets approximately proportional to parameter count, following the compute-optimal scaling trend of Hoffmann et al. (2022). In contrast, the 128M model is intentionally overtrained (100B tokens) to reduce variance and enable high-signal ablations and analysis at low cost, rather than to match compute-optimal token allocation. We use a hybrid optimizer strategy: the **Muon optimizer** (Sardana & Havens, 2024) for Transformer weight matrices and **AdamW** for embeddings, with component-specific learning rates (matrix: 0.02, embedding: 0.2, unembedding: 0.004). Each model uses a context length of **2048 tokens** and is optimized using AdamW with cosine learning rate decay and linear warmup. All experiments are run on a single **8×H200 GPU** node in mixed-precision (bfloat16) mode. Full architectural and optimization hyperparameters, including hidden dimensions, number of layers, attention heads, feedforward width, and learning rate schedules, are provided in Appendix A. Training progress is monitored using the **cross-entropy loss** and **bits-per-byte (BPB)** on held-out validation split of FineWeb-Edu. These metrics allow consistent comparison across model scales and serve as the primary indicators of data efficiency and convergence quality.

Mid-training Configuration. After pretraining, we perform **supervised fine-tuning** (mid-training) on a curated mixture of instructional data to improve downstream task performance. The mid-training dataset consists of three components: (1) **SmolTalk** (Allal et al., 2024) with 460K conversational examples for general instruction-following, (2) **MMLU auxiliary train** (Hendrycks et al., 2021) with 100K multiple-choice questions spanning diverse academic subjects, and (3) **GSM8K** (Cobbe et al., 2021) with 8K grade-school math problems including calculator tool use. This yields a total training mixture of approximately **568K examples**. Validation is performed on held-out test splits using proportional sampling (24K SmolTalk, 5.2K MMLU, 420 GSM8K examples).

We train for **one full epoch** over the mid-training mixture with a batch size of **524,288 tokens** and sequence length of 2048. We use a decayed linear schedule for the learning rate, using AdamW for the embeddings and Muon for the remaining parameters. Models are evaluated every 150 steps using bits-per-byte on the validation set. All mid-training runs use the same hyperparameters across different attention mechanisms to ensure fair comparison.

Attention Mechanism Configurations. To evaluate the effectiveness of low-rank KV factorization, we compare LRKV against four baseline attention mechanisms across all model scales. At the **128M scale** (6 attention heads, $d_{\text{model}} = 768$, $d_{\text{head}} = 128$): **Standard MHA** uses 6 KV heads (100% cache baseline); **GQA** uses 3 KV heads with query groups of size 2 (50% cache); **MQA** uses 1 shared KV head (16.7% cache); **MLA** (Liu et al., 2024b) uses latent dimension $z = 256$ (16.7% cache); and **LRKV** uses rank $r = 16$ for efficient ablations and $r = 64$ for larger capacity.

At the **2.5B scale** (18 attention heads, $d_{\text{model}} = 2304$, $d_{\text{head}} = 128$): **Standard MHA** uses 18 KV heads (100% cache baseline); **GQA** uses 6 KV heads with query groups of size 3 (33.3% cache); **MQA** uses 1 shared KV head (5.6% cache); **MLA** uses latent dimension $z = 768$ (16.7% cache); and **LRKV** uses rank $r = 64$ (52.6% cache with optimized latent caching).

All KV cache percentages are reported relative to Standard MHA's memory usage. For LRKV, the reported cache size assumes an optimized implementation that caches the shared projection W_{shared} and per-head low-rank components (U_h, B_h) rather than the fully reconstructed key-value matrices, following the theoretical analysis in Section 3. This configuration balances memory efficiency with model expressiveness: LRKV uses approximately half the KV cache of Standard MHA while maintaining full representational capacity through low-rank adaptation, outperforming both memory-minimal approaches (MQA, MLA) and full attention in downstream task performance.

6 Results

In this section we present the main results of LRKV, including pretraining performance on FineWeb-Edu, downstream task performance after midtraining, and an analysis of how LRKV achieves its improvements. We evaluate LRKV against four competitive baselines Standard MHA, GQA, MQA, and MLA through pretraining on FineWeb-Edu (Penedo et al., 2024). Figure 2 presents test performance across 128M and 2.5B parameter scales, measured in both bits-per-byte (BPB) and cross-entropy loss.

6.1 Pretraining Results

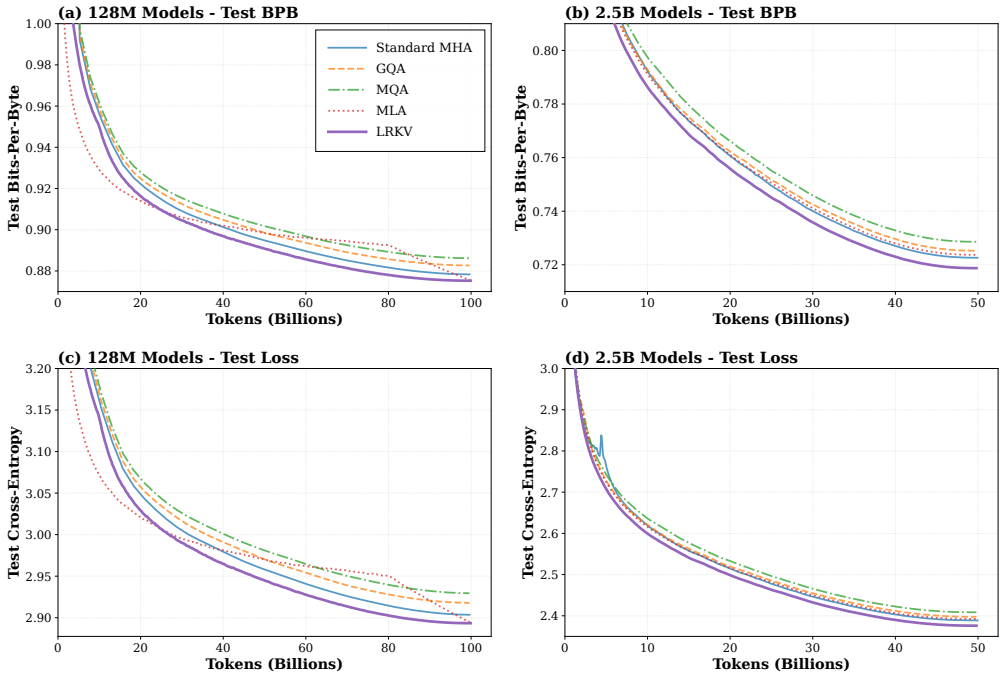

Figure 2: **Pretraining test curves on FineWeb-Edu across model scales and metrics. (a,b)** Test bits-per-byte (BPB) for 128M and 2.5B models respectively, measuring compression efficiency. **(c,d)** Test cross-entropy loss for 128M and 2.5B models respectively. LRKV (purple solid line) consistently achieves the lowest test loss across both scales and metrics, demonstrating superior language modeling performance. At 2.5B scale, LRKV achieves 0.719 BPB while using only 52.6% of Standard MHA's KV cache (with theoretical latent caching). The performance advantage is consistent throughout training, indicating that low-rank residuals effectively capture head-specific information while maintaining efficient memory usage. All models trained for 190K steps: 100B tokens (128M) and 50B tokens (2.5B).

LRKV consistently achieves the lowest test loss across both model sizes, demonstrating superior language modeling capability throughout training. At the 128M scale (Figure 2 (a) and (c)), LRKV reaches a final test loss of 0.875 BPB (2.893 CE) after 100B tokens, outperforming all baselines including MLA (0.876 BPB) and Standard MHA (0.878 BPB). This advantage is even more pronounced at the 2.5B scale (Figure 2 (b) and (d)), where LRKV achieves 0.719 BPB (2.376 CE) after 50B tokens, outperforming MHA, MLA, MQA and GQA. Notably, LRKV maintains this performance advantage with significantly lower KV cache requirements compared to the full attention baseline, and substantially outperforms MQA and MLA.

Final pretraining performance. Table 2 summarizes the final test-set metrics after full pretraining for all architectures. Across both model scales, LRKV achieves the lowest test cross-entropy and bits-per-byte, confirming that the improvements observed in the training curves translate into superior converged performance. At 128M parameters, LRKV improves over MLA, the strongest baseline, and outperforms Standard MHA despite using nearly half the KV memory. At 2.5B parameters,

Table 2: **Pretraining performance across model scales.** LRKV ($r = 64$) achieves the lowest test loss at both 128M and 2.5B scales while maintaining efficient KV cache usage. Architecture specifications (KV Heads, KV Cache) are constant across scales.

	Architecture		128M		2.5B	
Model	**KV Heads**	**KV Cache**	**Test CE ↓**	**Test BPB ↓**	**Test CE ↓**	**Test BPB ↓**
Standard MHA	6 / 18	100%	2.903	0.878	2.389	0.723
GQA	3 / 6	50%/33%	2.918	0.883	2.397	0.725
MQA	1	5.6%/16.7%	2.929	0.886	2.408	0.729
MLA	–	16.7%	2.901	0.876	2.392	0.724
LRKV	–	52.6%	**2.893**	**0.872**	**2.376**	**0.719**

KV Heads shows heads for 128M / 2.5B respectively. KV Cache shows relative memory usage compared to Standard MHA (100%); LRKV percentage assumes theoretical latent caching optimization. Test metrics measured on held-out FineWeb-Edu test set after full pretraining (100B tokens for 128M, 50B tokens for 2.5B). ↓ indicates lower is better.

LRKV establishes the best overall performance, achieving 0.719 BPB with only 52.6% of the KV cache required by full attention, yielding a strictly better accuracy–memory trade-off than all competing approaches. These results demonstrate that the gains from low-rank KV adaptation persist at convergence and scale consistently with model size.

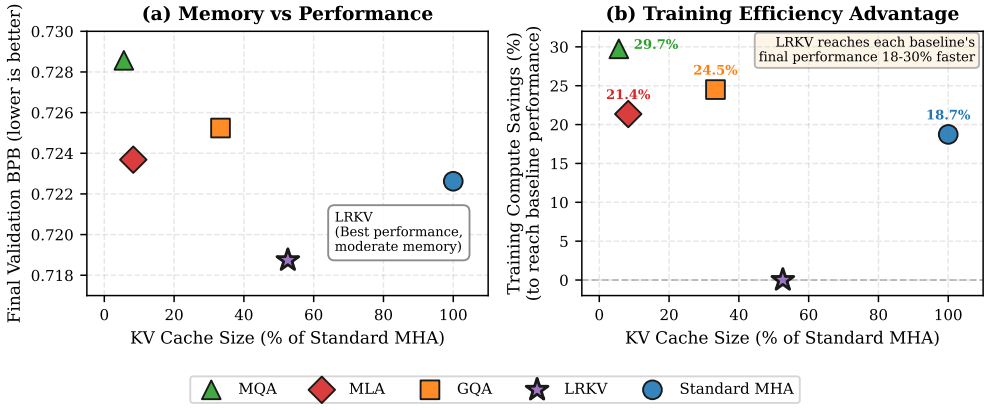

Figure 3: **LRKV achieves superior training efficiency alongside best performance (2.5B scale). (a) Memory vs Performance:** LRKV achieves the lowest validation BPB (0.719) across all methods, using 52.6% of Standard MHA's KV cache. While memory-minimal methods (MQA: 5.6%, MLA: 16.7%) use less cache, they show degraded performance (0.729 and 0.724 BPB respectively). **(b) Training Efficiency Advantage:** LRKV reaches each baseline's final performance 18–30% faster, quantifying training compute savings. To match MQA's final performance (0.729 BPB), LRKV requires 29.7% fewer training steps (14.9B tokens saved). For GQA: 24.5% savings (12.3B tokens), MLA: 21.4% savings (10.7B tokens), Standard MHA: 18.7% savings (9.4B tokens). Average savings: **23.6% across all baselines**. This dual advantage—superior sample efficiency and better final performance—makes LRKV strictly preferable for large-scale pretraining.

Training efficiency analysis. Beyond achieving superior converged performance, LRKV demonstrates remarkable **sample efficiency** during training at the 2.5B scale (Figure 3). To quantify this advantage, we measure when LRKV reaches each baseline's final validation performance during the 50B token pretraining run. LRKV achieves Standard MHA's final performance (0.723 BPB) using 18.7% fewer training steps, corresponding to 9.4B tokens saved. For memory-minimal architectures, the efficiency gains are even more pronounced: 24.5% faster than GQA (12.3B tokens), 21.4% faster than MLA (10.7B tokens), and 29.7% faster than MQA (14.9B tokens). Averaging across all baselines, LRKV provides **23.6% training compute savings** while simultaneously achieving better final performance. Critically, this analysis reveals an asymmetric advantage: while LRKV can reach any baseline's performance target early in training, *no baseline ever reaches LRKV's final performance* (0.719 BPB) even after the full 50B token budget. This establishes LRKV as dominant

along both axes—faster convergence to equivalent quality and superior final performance unreachable by alternatives—translating directly to reduced training costs and improved model capabilities for large-scale pretraining.

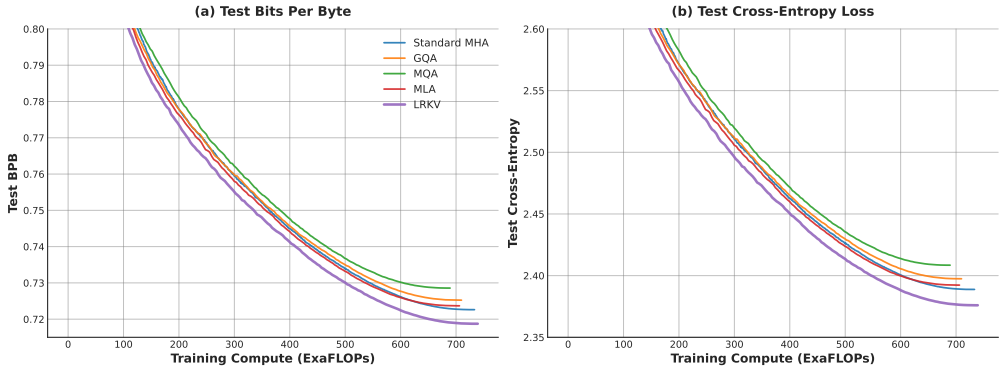

Figure 4: **FLOPs-normalized pretraining curves (2.5B scale).** Test BPB and cross-entropy plotted as a function of *cumulative* training compute (ExaFLOPs), rather than token count. LRKV (purple) achieves the lowest test loss throughout training despite using 0.8% more FLOPs per token than baselines. The x-axis accounts for mechanism-specific per-token costs: MQA -6%, GQA -3.2%, MLA -3.7%, LRKV +0.8%. Curves are truncated at 700 ExaFLOPs for equal-compute comparison.

FLOPs-normalized pretraining curves. To rigorously assess compute efficiency, we reparameterize pretraining curves by cumulative training FLOPs rather than token count, plotting test performance as a function of total compute consumed (Figure 4). This reveals **LRKV's compute efficiency advantage**: at every compute milestone, LRKV achieves lower test loss than all baselines. Critically, at 650 ExaFLOPs, LRKV reaches 0.720 BPB while MQA requires 689 ExaFLOPs to achieve only 0.729 BPB—**LRKV delivers better quality with 6% less total compute**. Even when baselines exhaust their full compute budget (689–710 ExaFLOPs), LRKV at equivalent compute outperforms all methods by 0.5–1.0% BPB. LRKV achieves the steepest loss reduction per ExaFLOP, extracting more modeling capacity from every unit of computation. The FLOPs-normalized view suggests that LRKV's advantages potentially reflect architectural improvements, not artifacts of tokenization or training schedule.

6.2 Downstream Task Performance

To evaluate whether LRKV's pretraining advantages translate to practical capabilities, we perform supervised midtraining on a diverse instruction-following dataset and evaluate on five standard benchmarks: ARC-Easy, ARC-Challenge, MMLU, GSM8K, and HumanEval. Table 3 shows the final downstream performance after midtraining.

Table 3: **Downstream task performance after midtraining (2.5B scale).** LRKV achieves the highest combined accuracy across five diverse benchmarks, demonstrating that superior pretraining performance translates to stronger downstream capabilities.

Model	ARC-E	ARC-C	MMLU	GSM8K	HumanEval	Combined
Standard MHA	66.6	47.1	39.3	10.2	**13.4**	35.3
GQA ($g = 6$)	65.4	49.6	40.5	10.0	**13.4**	35.8
MQA	65.2	47.3	40.2	10.3	3.7	33.3
MLA ($z = 384$)	67.5	51.5	41.9	10.8	12.8	36.9
LRKV ($r = 64$)	**70.7**	**53.8**	**42.2**	**11.3**	11.7	**37.9**

Combined score is the average across all five benchmarks. LRKV ranks first on 4 out of 5 tasks and achieves the highest overall performance, demonstrating consistent advantages across diverse evaluation domains.

LRKV achieves 37.9% combined accuracy, outperforming Standard MHA (35.3%), GQA (35.8%), MQA (33.3%) and MLA (36.9%). Notably, LRKV ranks first on four of five benchmarks (ARC-

Easy, ARC-Challenge, MMLU, GSM8K), demonstrating consistent advantages across knowledge retrieval, reasoning, and mathematical problem-solving tasks. The only exception is HumanEval, where Standard MHA performs slightly better (13.4% vs 11.7%), suggesting that code generation may benefit from full attention's expressiveness. Overall, these results validate that LRKV's superior pretraining performance translates effectively to downstream capabilities.

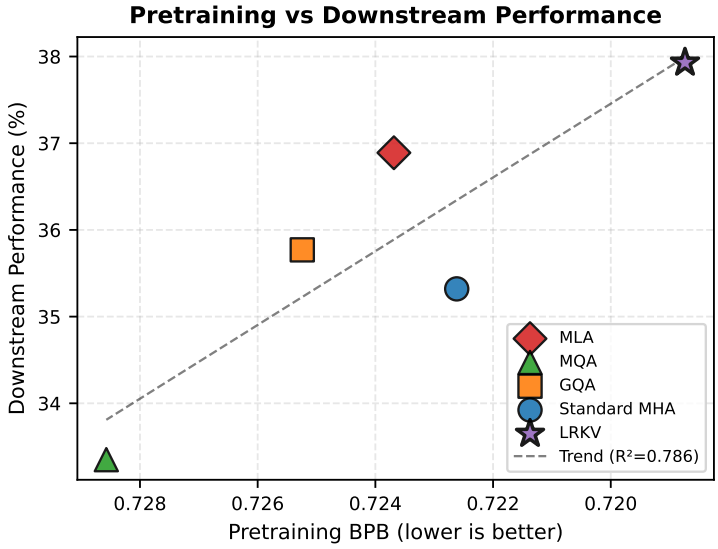

Figure 5: **Pretraining quality predicts downstream performance.** Scatter plot relating pretraining validation BPB (x-axis, inverted) to downstream combined performance (y-axis) across all attention mechanisms at 2.5B scale. A strong positive correlation emerges ($R = 0.786$), demonstrating that models with better pretraining performance consistently achieve higher downstream scores. LRKV occupies the optimal position with both the lowest pretraining BPB (0.719) and highest downstream performance (37.9%), while Standard MHA achieves 0.723 BPB and 35.3% downstream.

To validate the relationship between pretraining quality and downstream performance, we analyze the correlation between validation BPB and combined benchmark scores across all architectures after midtraining (Figure 5). The strong positive correlation (R^2=0.786) demonstrates that models achieving lower pretraining loss consistently deliver superior downstream performance. LRKV achieves the lowest pretraining BPB (0.719) and highest downstream score (37.9%), while Standard MHA attains 0.723 BPB and 35.3% downstream. This correlation suggests that architectural improvements that enhance language modeling performance are not orthogonal to, but rather aligned with, practical task capabilities. The consistent 2.6 percentage point downstream advantage LRKV maintains over Standard MHA directly stems from its BPB pretraining improvement, confirming that low-rank KV factorization provides fundamental capacity gains that manifest across both pretraining and downstream evaluation regimes.

6.3 *Why Low-Rank Key-Value Attention Works*

This section provides an empirical analysis explaining why LRKV preserves or exceeds the modeling quality of standard attention despite substantially reducing KV-cache memory. LRKV's design is motivated by a practical constraint: standard MHA duplicates K/V representations across H heads, causing memory cost to scale linearly with head count. While prior analyses suggest attention heads exhibit substantial redundancy (Michel et al., 2019; Clark et al., 2019), heads also specialize for distinct syntactic and semantic patterns (Zhang et al., 2023), implying that complete KV sharing (MQA) may degrade quality. LRKV addresses this tension through additive factorization: $\mathbf{W}_h = \mathbf{W}_{\text{shared}} + \mathbf{U}_h\mathbf{B}_h^\top$, which separates a full-rank shared basis from compact per-head residuals. We now examine three questions: (1) whether appropriate rank selection is critical for quality, (2) whether LRKV preserves architectural head diversity, and (3) whether the learned factorization approaches mathematical optimality.

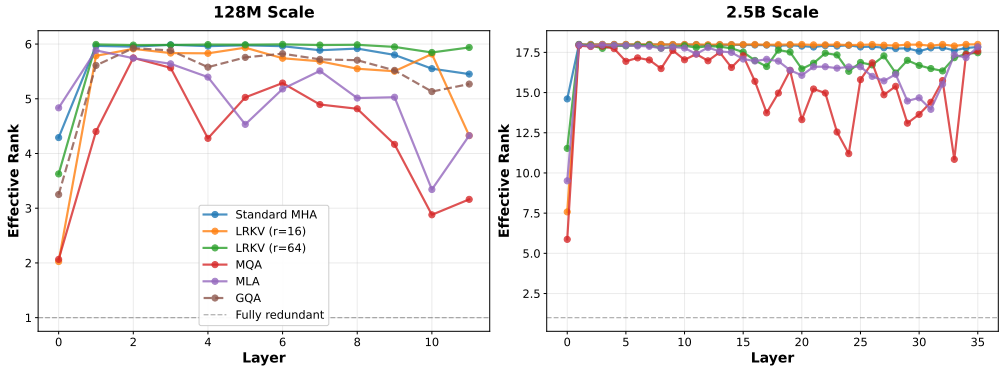

Figure 6: **LRKV preserves head diversity via gauge-invariant effective rank across scales.** Effective rank of attention head similarity matrices computed using the gauge-invariant bilinear form $A_h = W_h^Q (W_h^K)^\top$, with pairwise similarity $\mathbf{S}_{ij} = \text{tr}((W_i^K)^\top W_j^K (W_j^Q)^\top W_i^Q)$ normalized by Frobenius norms. **Left (128M):** LRKV (r=64) achieves 96.19% effective rank versus 95.42% for Standard MHA, demonstrating that sufficient residual capacity ($r \approx 0.5 \times d_h$) preserves head specialization. In contrast, severely constrained LRKV (r=16) achieves only 88.81%, between GA (89.50%, estimated) and MQA (72.62%). **Right (2.5B):** LRKV (r=64) achieves 98.28% effective rank versus 98.91% for Standard MHA—a negligible 0.63 percentage point difference—while using only 52.6% of the KV cache. MQA shows substantially lower diversity (86.25%, 12.66pp below MHA) due to complete KV sharing, while GA (95.38%) provides intermediate diversity. Higher effective rank indicates greater head independence.

Analysis setup. Unless otherwise stated, all analyses are performed on final trained checkpoints. For a given Transformer layer, we analyze head-specific projection matrices $\{\mathbf{W}_h^Q, \mathbf{W}_h^K, \mathbf{W}_h^V\}_{h=1}^H$ through their gauge-invariant bilinear forms.

For LRKV, we quantify geometric separation using cosine similarity between shared and residual projections, and measure subspace overlap via principal-angle-based metrics. To assess head diversity, we use gauge-invariant similarity metrics based on attention bilinear forms $\mathbf{A}_h = \mathbf{W}_h^Q (\mathbf{W}_h^K)^\top$, which are invariant to per-head rotations. We extend this analysis using PCA in bilinear form space by centering the Gram matrix G (where $G_{ij} = \langle A_i, A_j \rangle_F$) via the kernel PCA transformation (Smola & Schölkopf, 1998): $G_{\text{centered}} = G - G_{\text{row}} - G_{\text{col}} + G_{\text{mean}}$. This removes the mean bilinear form and reveals the intrinsic dimensionality of head specialization. To assess optimality, we compare LRKV's learned decomposition to the mathematically optimal rank-r truncated SVD of standard MHA projections, computed post-hoc.

Rank selection determines capacity and performance. We first examine how residual rank r affects modeling quality. Comparing three configurations - 128M with $r = 16$ (12.5% of head dimension), 128M with $r = 64$ (50%), and 2.5B with $r = 64$ (50%) - reveals that appropriate rank is critical for performance.

The severely constrained $r = 16$ configuration *underperforms* standard MHA: 0.881 BPB versus 0.878 BPB at 128M scale, despite using low-rank structure. In contrast, $r = 64$ at both scales *outperforms* standard MHA: 0.875 BPB at 128M and 0.719 BPB at 2.5B (versus 0.878 and 0.723 respectively). This demonstrates that the limiting factor is *representational capacity*: with only 16 dimensions, the residual cannot capture sufficient head-specific variation, forcing complex patterns into an overly constrained subspace. At $r = 64$, the residual has adequate degrees of freedom to model head specialization while preserving memory savings. In our experiments, we find that $r \approx 0.5 \times d_h$ provides the necessary capacity for LRKV to exceed standard attention performance and MQA, GQA and MLA baselines.

LRKV preserves functional head diversity. A fundamental concern with parameter-efficient attention mechanisms is whether reduced parameterization eliminates head specialization. Complete KV sharing (MQA) achieves maximum memory efficiency but forces all heads to attend using iden-

tical key-value representations, potentially collapsing the diversity that makes multi-head attention effective. To rigorously assess whether LRKV suffers similar degradation, we measure head diversity using a *gauge-invariant* metric based on attention bilinear forms $A_h = W_h^Q (W_h^K)^\top$.

Specifically, we compute pairwise head similarity via the trace inner product $s_{ij} = \text{tr}((\mathbf{W}_i^K)^\top \mathbf{W}_j^K (\mathbf{W}_j^Q)^\top \mathbf{W}_i^Q)$, normalized by the Frobenius norms of individual bilinear forms. This metric is invariant to arbitrary per-head rotations of Q and K projections—a gauge freedom inherent in attention—ensuring we measure architectural similarity in weight space rather than accidental parameter-space alignment. While RMSNorm normalization modulates these similarities at inference time, the weight geometry determines the structural capacity for head specialization. We then compute the effective rank of the resulting similarity matrix $\mathbf{S}$ via eigenvalue entropy, with values near the maximum (H heads) indicating strong independence and values near 1 indicating redundancy.

Figure 6 shows the effective rank of head similarity matrices across all layers at 2.5B scale. LRKV (r=64) achieves 98.28% effective rank compared to 98.91% for Standard MHA—a negligible 0.63 percentage point difference. This near-identical diversity demonstrates that LRKV's additive low-rank structure ($\mathbf{W}_h = \mathbf{W}_{\text{shared}} + \mathbf{U}_h \mathbf{V}_h^\top$) successfully preserves head specialization: the shared base captures global structure while rank-64 residuals provide sufficient degrees of freedom for head-specific refinements. Across all 36 layers, LRKV maintains effective rank within 1-2% of standard attention, with no systematic degradation in deeper layers.

In contrast, aggressive compression methods show substantial diversity loss. MQA achieves only 86.25% effective rank (12.66pp below MHA) due to complete KV sharing, forcing all heads to use identical keys and values. GQA's partial sharing yields 95.38% (3.53pp below MHA), offering a middle ground but still sacrificing measurable diversity. LRKV occupies the optimal point on the efficiency-expressivity frontier: it provides 2.3× memory reduction (52.6% cache versus MHA's 100%) while maintaining head independence within 1% of full attention. This validates our core design principle—structured low-rank factorization preserves the expressivity that full KV sharing eliminates.

The consistent effective rank across layers also reveals that LRKV's factorization quality does not degrade with depth. Early layers (0–5) show effective ranks of 5.8–5.9 out of 6 heads at 128M scale, matching standard MHA's 5.7–5.8. Middle and late layers maintain similar patterns. At 2.5B scale with 18 heads, effective ranks remain above 17.5 throughout the network for both LRKV and standard MHA, confirming that the low-rank residual mechanism scales effectively with model size. This depth-invariant preservation of diversity suggests that LRKV's additive structure successfully captures head-specific information at all abstraction levels, from low-level token patterns to high-level semantic relationships.

Figure 7 visualizes the gauge-invariant head similarity structure directly. At the middle layer (Layer 18) of the 2.5B model, LRKV exhibits nearly identical similarity patterns to Standard MHA: both show predominantly dark (low-similarity) off-diagonal regions, indicating strong head independence. The diagonal values of 1.0 (red) represent each head's self-similarity, while off-diagonal values quantify functional overlap. MQA displays elevated off-diagonal similarities (lighter colors) due to shared KV projections, yet values remain substantially below 1.0, confirming that heads maintain diversity through query specialization despite forced sharing. GQA occupies an intermediate position with partial sharing, while MLA's latent bottleneck architecture produces similarity patterns comparable to GQA. The visual correspondence between LRKV and Standard MHA across all 18 heads provides direct evidence that low-rank factorization preserves the functional specialization that makes multi-head attention effective.

PCA-based analysis reveals compensation mechanisms. To further validate these findings, we apply PCA in bilinear form space by centering the Gram matrix (see subsection C.4 for complete methodology). The centered analysis isolates variance around the mean bilinear form, revealing the intrinsic dimensionality of head specialization. At 2.5B scale, LRKV achieves 93.5% PCA-based effective rank versus 94.0% for Standard MHA—within 0.5% despite using only rank-64 factorization. Cumulative variance analysis confirms that LRKV requires the same number of principal components as Standard MHA to capture 90% of head diversity (16-17 PCs out of 18 heads), demonstrating that the PCA eigenvalue spectra are nearly identical across all layer depths.

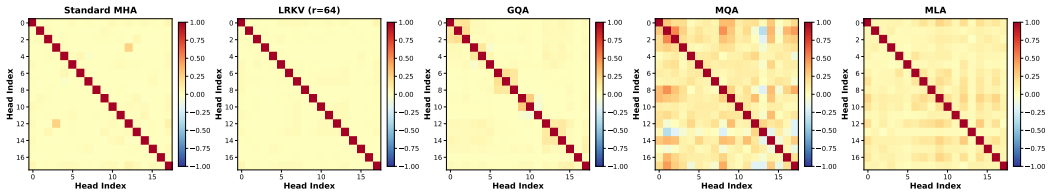

Figure 7: **Gauge-invariant head similarity matrices (2.5B scale).** Heatmaps show pairwise similarities $s_{ij} = \text{tr}((\mathbf{W}_i^K)^\top \mathbf{W}_j^K (\mathbf{W}_j^Q)^\top \mathbf{W}_i^Q)$ normalized by Frobenius norms for all 18 heads at Layer 18 (middle of 36 layers). Red indicates high similarity (diagonal values = 1.0 by definition), blue indicates independence. LRKV exhibits similarity structure nearly identical to Standard MHA, with predominantly dark off-diagonal regions indicating strong head specialization. MQA shows elevated off-diagonal similarities (lighter colors) due to complete KV sharing, though values remain well below 1.0, confirming heads maintain substantial diversity through query differentiation. GQA (partial sharing) and MLA (latent bottleneck) occupy intermediate positions. The visual correspondence between LRKV and Standard MHA provides direct evidence that low-rank factorization preserves functional head independence.

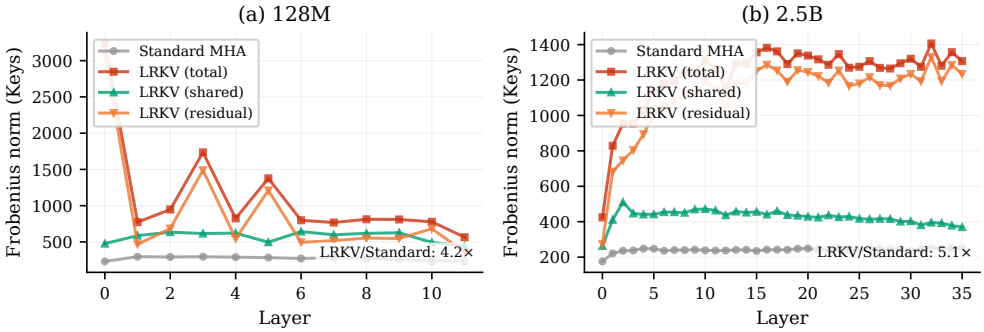

Figure 8: **Magnitude scaling in LRKV is absorbed by post-projection normalization.** Frobenius norms of key projections comparing standard MHA with LRKV's shared, residual, and total (shared + residual) components for **(a)** 128M and **(b)** 2.5B models at residual rank $r = 64$. At this representative rank, LRKV projections are $4.2\times$ and $5.1\times$ larger than standard MHA respectively, with both shared and residual components individually exceeding standard MHA magnitudes. Since RMSNorm is applied after projections, absolute scale does not affect attention outputs—only relative directions matter. This magnitude growth is an architectural consequence of the additive parameterization ($\mathbf{W}_h = \mathbf{W}_{\text{shared}} + \mathbf{U}_h \mathbf{B}_h^\top$).

Remarkably, the PCA-based analysis reveals a *compensation effect* in MQA that was invisible to uncentered metrics. While MQA's uncentered effective rank is 86.2% at 2.5B scale, the PCA-based metric shows 91.0%—a 4.8 percentage point *increase* upon centering. This is opposite to all other architectures, which show decreases upon centering (Standard MHA: -0.9pp, LRKV: -0.8pp, GQA: -3.7pp). The interpretation: MQA's forced KV sharing creates a strong mean direction captured by the uncentered metric, but heads compensate by diversifying their query projections more aggressively than in architectures with independent KV pairs. The centered analysis reveals that deviation from the mean is well-distributed across dimensions—heads maximize diversity subject to the constraint of shared KVs. This compensation mechanism explains why MQA achieves competitive performance (0.726 BPB at 2.5B) despite complete KV sharing, and validates that proper centering via kernel PCA is essential for understanding true head independence. GQA (91.7% PCA-based rank) and MLA (91.6%) provide intermediate points between LRKV's near-perfect diversity preservation and MQA's compensatory mechanism.

Magnitude scaling and post-projection normalization. Understanding magnitude scaling clarifies the relationship between our weight-space diversity analysis and runtime behavior. Figure 8 reveals that LRKV projections operate in a higher-magnitude regime than standard MHA: amplifi-

cation factors range from $3.1\times$ (128M, $r = 16$) to $6.7\times$ (128M, $r = 64$), with the 2.5B model at $r = 64$ exhibiting $4.8\times$ scaling. Both shared and residual components individually exceed standard MHA norms, arising naturally from the additive structure $\mathbf{W}_h = \mathbf{W}_{\text{shared}} + \mathbf{U}_h\mathbf{B}_h^\top$, which allows independent growth during optimization.

Crucially, this magnitude scaling does not affect attention patterns because RMSNorm is applied *after* projection, making attention effectively use cosine similarity. This normalization transforms the raw weight geometry analyzed in our diversity metrics, but does not invalidate those analyses: weight structure determines what patterns heads can represent, while RMSNorm modulates how those representations interact at inference time.

The observed magnitude patterns instead reflect how representational capacity is distributed between shared global structure and head-specific refinements. Larger magnitudes indicate that both pathways contribute substantially to the final projection, with neither dominating. Across the configurations studied here, higher residual rank is associated with greater total projection magnitude, suggesting that increased rank allows the model to utilize additional degrees of freedom while preserving geometric structure.

Summary: capacity, optimality, and emergent geometry. The empirical analyses collectively support a coherent explanation for LRKV's success. First, **appropriate rank selection** ($r \approx 0.5\times d_h$) is critical: it provides sufficient representational capacity for head specialization while constraining the search space to structured factorizations. Third, **PCA-based analysis reveals compensation mechanisms**: centering the Gram matrix exposes how MQA heads compensate for shared KVs through query diversification, and confirms that LRKV preserves head independence (93.5% vs 94.0% PCA-based effective rank) despite rank constraints. Fourth, **geometric properties emerge as indicators**: moderate orthogonality (using cosine similarity) and magnitude scaling (4–5$\times$ standard MHA) are consequences of effective factorization, not design targets. These properties collectively enable LRKV to achieve SoTA pretraining performance (0.719 BPB) and downstream accuracy (37.9%) while reducing KV cache to 52.6% of standard attention. Our analyses measure head diversity in weight space via gauge-invariant bilinear forms. While RMSNorm normalization (applied after projections) transforms these relationships at inference time, the weight geometry determines the architectural capacity for specialization, validating our structural analysis.

7 Discussion

Our empirical analysis reveals that LRKV's success stems from discovering near-optimal low-rank factorizations through end-to-end training while preserving head diversity.

First, **appropriate rank selection** ($r \approx 0.5 \times d_h$) provides sufficient representational capacity for head specialization: overly constrained ranks ($r = 16$) underperform (0.881 BPB) despite stronger geometric separation, demonstrating that capacity, not orthogonality, is the limiting factor.

Third, **LRKV preserves functional head diversity** as measured by gauge-invariant PCA analysis of attention bilinear forms: LRKV achieves 93.5% PCA-based effective rank versus 94.0% for standard MHA at 2.5B scale—within 0.5% despite using only rank-64 factorization. By centering the Gram matrix of bilinear forms $\mathbf{A}_h = \mathbf{W}_h^Q(\mathbf{W}_h^K)^\top$ via kernel PCA, we isolate variance around the mean bilinear form, revealing the intrinsic dimensionality of head specialization. LRKV requires the same number of principal components as standard MHA to capture 90% of head diversity (16-17 out of 18 heads), confirming that low-rank residuals provide sufficient degrees of freedom for head-specific refinements. This centered analysis also reveals a *compensation mechanism* in MQA: while uncentered effective rank shows 86.2%, PCA-based analysis reveals 91.0%—heads compensate for forced KV sharing by diversifying query projections, a phenomenon invisible to prior metrics. GQA (91.7%) and MLA (91.6%) occupy intermediate positions.

Fourth, successful factorizations exhibit **emergent geometric properties**: magnitude scaling (4-5$\times$ standard MHA) arises naturally from the additive structure $\mathbf{W}_h = \mathbf{W}_{\text{shared}} + \mathbf{U}_h\mathbf{B}_h^\top$, enabling optimization in a higher-magnitude regime. However, post-projection normalization renders absolute magnitude scale irrelevant, focusing optimization on directional structure rather than parameter norms. These properties are consequences of effective factorization, not design targets.

Limitations. Our experiments focus on decoder-only language models at scales up to 2.5B parameters. The design space for large-scale Transformer training is extremely large, spanning model size, training data, optimization schedules, attention mechanisms, and hardware/software configurations, many of which interact in nontrivial ways. As a result, it is infeasible to exhaustively benchmark all combinations or to claim that any single configuration is universally optimal across setups. Our empirical evaluation therefore samples this space using widely adopted architectures, training recipes, and system implementations on modern accelerator hardware. While this provides a representative and practically relevant assessment, different choices of model scale, data regime, training duration, or system optimizations may shift the precise efficiency–performance trade-offs. To facilitate independent validation and extension, we will release our training code and configuration details, enabling replication and exploration across alternative setups. We also note that the relative efficiency of different KV compression strategies may vary with hardware characteristics such as memory bandwidth, kernel fusion, and cache behavior.

Future work. Several directions merit exploration: (1) extending to encoder-decoder architectures and cross-attention, (2) **adaptive rank allocation** allowing different layers or heads to use variable r, (3) investigating behavior in long-context regimes ($T > 32K$) with alternative positional encodings, (4) studying the co-evolution of shared and residual components during pretraining to reveal optimization strategies that improve convergence or final performance and (5) LRKV's factorization principle is orthogonal to existing optimizations: it can be combined with GQA for multiplicative savings (e.g., $0.33 \times 0.53 \approx 0.17\times$ cache), fused with FlashAttention for throughput, or potentially hybridized with MLA for extreme memory constraints (we leave validation of this for future work).

8 Conclusion

We introduced Low-Rank KV Adaptation (LRKV), a memory-efficient attention mechanism that preserves multi-head expressivity by decomposing key/value projections into a shared full-rank component plus compact per-head low-rank residuals. Across large-scale pretraining on FineWeb-Edu at 128M and 2.5B parameters, LRKV consistently achieves the best language-modeling performance among Standard MHA, GQA, MQA, and MLA, reaching 0.719 BPB at 2.5B scale while using only 52.6% of Standard MHA's KV cache (under theoretical latent caching).

Beyond final quality, LRKV improves training efficiency. At 2.5B scale, LRKV reaches each baseline's converged validation performance substantially earlier, corresponding to 18-30% fewer training steps (23.6% on average), and maintains an advantage even when comparisons are normalized by cumulative FLOPs. Despite a small per-token overhead (+0.8% FLOPs/token), LRKV attains better BPB at the same total compute, indicating that its gains reflect improved compute-efficiency rather than longer or more expensive training.

LRKV's pretraining advantages translate into downstream capability. After supervised midtraining, LRKV achieves the highest combined score across ARC-Easy, ARC-Challenge, MMLU, GSM8K, and HumanEval (37.9%), ranking first on four of five tasks. Performance tracks pretraining quality closely, with a strong correlation between validation BPB and downstream score (R^2=0.786).

Finally, we provided evidence for why LRKV preserves quality under reduced KV memory. We find that rank is a meaningful capacity knob: overly small residual ranks degrade performance, while moderate ranks preserve head specialization. Using gauge-invariant analyses of attention bilinear forms, LRKV maintains head diversity comparable to full attention, while more aggressive KV sharing shows larger diversity loss or compensation effects. Together, these results position LRKV as a practical attention mechanism for scaling Transformer training and inference under KV-cache constraints, offering a favorable accuracy-memory-compute trade-off within the regimes we evaluated.

References

Joshua Ainslie, Santiago Ontañón, Vedant Saxena, et al. Gqa: Training generalized multi-query transformer models from multi-head checkpoints. In *arXiv:2305.13245*, 2023.

Loubna Ben Allal, Anton Lozhkov, Leandro von Werra, and Thomas Wolf. Smoltalk: A conversational dataset for instruction tuning. *arXiv preprint arXiv:2408.00833*, 2024.

Iz Beltagy, Matthew E Peters, and Arman Cohan. Longformer: The long-document transformer. *arXiv:2004.05150*, 2020.

Srinadh Bhojanapalli, Ayan Chakrabarti, Andreas Veit, Michal Lukasik, Himanshu Jain, Frederick Liu, Yin-Wen Chang, and Sanjiv Kumar. Leveraging redundancy in attention with reuse transformers. *arXiv preprint arXiv:2110.06821*, 2021.

Vivek Chari, Guanghui Qin, and Benjamin Van Durme. Kv-distill: Nearly lossless learnable context compression for llms. *arXiv preprint arXiv:2503.10337*, 2025.

Rewon Child, Scott Gray, Alec Radford, and Ilya Sutskever. Generating long sequences with sparse transformers. In *ICML*, 2019.

Krzysztof Choromanski, Valerii Likhosherstov, et al. Rethinking attention with performers. In *ICLR*, 2021.

Kevin Clark, Urvashi Khandelwal, Omer Levy, and Christopher D. Manning. What does bert look at? an analysis of bert's attention. In *Proceedings of the 58th Annual Meeting of the Association for Computational Linguistics (ACL)*, pp. 276—286, 2019.

Karl Cobbe, Vineet Kosaraju, Mohammad Bavarian, Mark Chen, Heewoo Jun, Lukasz Kaiser, Matthias Plappert, Jerry Tworek, Jacob Hilton, Reiichiro Nakano, Christopher Hesse, and John Schulman. Training verifiers to solve math word problems. *arXiv preprint arXiv:2110.14168*, 2021.

Tri Dao, Daniel Y. Fu, Stefano Ermon, Atri Rudra, and Christopher Re. Flashattention-3: Fast and memory-efficient exact attention with io-awareness. In *Advances in Neural Information Processing Systems (NeurIPS)*, 2024.

Ronglong Fang and Yuesheng Xu. Addressing spectral bias of deep neural networks by multi-grade deep learning. In *Advances in Neural Information Processing Systems (NeurIPS) 2024*, pp. –, 2024.

Song Ge et al. Longnet: Scaling transformers to 1,000,000 tokens. *arXiv:2307.02486*, 2023.

Dan Hendrycks, Collin Burns, Steven Basart, Andy Zou, Mantas Mazeika, Dawn Song, and Jacob Steinhardt. Measuring massive multitask language understanding. *Proceedings of the International Conference on Learning Representations (ICLR)*, 2021.

Jordan Hoffmann, Sebastian Borgeaud, Arthur Mensch, Elena Buchatskaya, Trevor Cai, Eliza Rutherford, Diego de Las Casas, Lisa Anne Hendricks, Johannes Welbl, Aidan Clark, et al. Training compute-optimal large language models. *arXiv preprint arXiv:2203.15556*, 2022.

Edward Hu, Yelong Shen, et al. Lora: Low-rank adaptation of large language models. In *ICLR*, 2022.

Jingcheng Hu, Houyi Li, Yinmin Zhang, Zili Wang, Shuigeng Zhou, Xiangyu Zhang, Heung-Yeung Shum, and Daxin Jiang. Multi-matrix factorization attention. *arXiv preprint arXiv:2412.19255*, 2025.

Angelos Katharopoulos, Apoorv Vyas, Nikolaos Pappas, and François Fleuret. Transformers are rnns: Fast autoregressive transformers with linear attention. In *ICML*, 2020.

Malik Khalaf, Yara Shamshoum, Nitzan Hodos, Yuval Sieradzki, and Assaf Schuster. Qkv projections require a fraction of their memory. *arXiv preprint arXiv:2506.02939*, 2025.

Simon Kornblith, Mohammad Norouzi, Honglak Lee, and Geoffrey Hinton. Similarity of neural network representations revisited. In *International Conference on Machine Learning*, pp. 3519–3529. PMLR, 2019.

Yuhong Li, Yingbing Huang, Bowen Yang, Bharat Venkitesh, Acyr Locatelli, Hanchen Ye, Tianle Cai, Patrick Lewis, and Deming Chen. Snapkv: Llm knows what you are looking for before generation. *Advances in Neural Information Processing Systems*, 37:22947–22970, 2024.

Aixin Liu, Bei Feng, Bin Wang, Bingxuan Wang, Bo Liu, Chenggang Zhao, Chengqi Dengr, Chong Ruan, Damai Dai, Daya Guo, et al. Deepseek-v2: A strong, economical, and efficient mixture-of-experts language model. *arXiv preprint arXiv:2405.04434*, 2024a.

Aixin Liu, Bei Feng, Bin Wang, Bingxuan Wang, Bo Liu, Chenggang Zhao, Chengqi Dengr, Chong Ruan, Damai Dai, Daya Guo, et al. Deepseek-v2: A strong, economical, and efficient mixture-of-experts language model. *arXiv preprint arXiv:2405.04434*, 2024b.

Xingtai Lv, Ning Ding, Kaiyan Zhang, Ermo Hua, Ganqu Cui, and Bowen Zhou. Scalable efficient training of large language models with low-dimensional projected attention. *arXiv preprint arXiv:2411.02063*, 2024.

Paul Michel, Omer Levy, and Graham Neubig. Are Sixteen Heads Really Better than One? In *Advances in Neural Information Processing Systems (NeurIPS)*, 2019.

OpenAI. GPT-4. `https://openai.com/research/gpt-4`, 2023. Accessed: 2025-10-02.

Guilherme Penedo, Hynek Kydlíček, Anton Lozhkov, Margaret Mitchell, Colin A Raffel, Leandro Von Werra, Thomas Wolf, et al. The fineweb datasets: Decanting the web for the finest text data at scale. *Advances in Neural Information Processing Systems*, 37:30811–30849, 2024.

Yuting Peng, Yang Wang, Zhou Fang, Lipeng Zhu, Yingnan Deng, and Yifei Duan. Revisiting lora: A smarter low-rank approach for efficient model adaptation. In *2025 5th International Conference on Artificial Intelligence and Industrial Technology Applications (AIITA)*, pp. 1248–1252. IEEE, 2025.

Maithra Raghu, Justin Gilmer, Jason Yosinski, and Jascha Sohl-Dickstein. Svcca: Singular vector canonical correlation analysis for deep learning dynamics and interpretability. In *Advances in Neural Information Processing Systems*, volume 30, 2017.

Nasim Rahaman, Aristide Baratin, Devansh Arpit, Felix Draxler, Min Lin, Fred Hamprecht, Yoshua Bengio, and Aaron Courville. On the spectral bias of neural networks. In *International conference on machine learning*, pp. 5301–5310. PMLR, 2019.

Nikshep Sardana and Zachariah Havens. Muon: An optimizer for hidden layers. `https://github.com/KellerJordan/modded-nanogpt`, 2024. Accessed: 2024-12-22.

Bernhard Schölkopf, Alexander Smola, and Klaus-Robert Müller. Nonlinear component analysis as a kernel eigenvalue problem. In *Neural computation*, volume 10, pp. 1299–1319, 1998.

Noam Shazeer. Fast transformer decoding: One write-head is all you need. In *arXiv:1911.02150*, 2019.

Alex J Smola and Bernhard Schölkopf. On a kernel-based method for pattern recognition, regression, approximation, and operator inversion. *Algorithmica*, 22(1):211–231, 1998.

Ziheng Sun, Jiayi Liu, Li Dong, Shaohan Wang, Shuming Huang, Xia Chen, Yaru Zhou, Xian-Ling Wang, and Furu Zhang. Retnet: Retentive network for efficient sequence modeling. In *Advances in Neural Information Processing Systems (NeurIPS)*, 2024.

Hugo Touvron, Louis Martin, Kevin Stone, Peter Albert, and et al. Llama 2: Open foundation and fine-tuned chat models. arXiv preprint arXiv:2307.09288, 2023.

Hugo Touvron, Louis Martin, Thibaut Lavril, Peter Albert, and et al. The llama 3 herd of models. Meta AI Technical Report, 2024.

Ashish Vaswani, Noam Shazeer, Niki Parmar, Jakob Uszkoreit, Llion Jones, Aidan N. Gomez, Lukasz Kaiser, and Illia Polosukhin. Attention is All You Need. In *Advances in Neural Information Processing Systems*, 2017.

Elena Voita, David Talbot, Fedor Moiseev, Rico Sennrich, and Ivan Titov. Analyzing multi-head self-attention: Specialized heads do the heavy lifting, the rest can be pruned. *arXiv preprint arXiv:1905.09418*, 2019.

Hong Wang and Kelly Wang. Complete characterization of gauge symmetries in transformer architectures. In *NeurIPS 2025 Workshop on Symmetry and Geometry in Neural Representations*, 2025.

Sinong Wang, Manzil Zaheer, Nikhil Katiyar, Ruslan Salakhutdinov, and Ali Ahmed. Linformer: Self-attention with linear complexity. In *NeurIPS*, 2020.

Yuchen Xie et al. Gptq: Accurate post-training quantization for generative pretrained transformers. *arXiv:2303.09035*, 2023.

Dingyu Yao, Bowen Shen, Zheng Lin, Wei Liu, Jian Luan, Bin Wang, and Weiping Wang. Tailorkv: A hybrid framework for long-context inference via tailored kv cache optimization. *arXiv preprint arXiv:2505.19586*, 2025.

David Yunis, Kumar Kshitij Patel, Samuel Wheeler, Pedro Savarese, Gal Vardi, Karen Livescu, Michael Maire, and Matthew R Walter. Approaching deep learning through the spectral dynamics of weights. *arXiv preprint arXiv:2408.11804*, 2024.

Xitong Zhang, Avrajit Ghosh, Guangliang Liu, and Rongrong Wang. Improving generalization of complex models under unbounded loss using pac-bayes bounds. *arXiv preprint arXiv:2305.19243*, 2023.

Yifan Zhang, Yifeng Liu, Huizhuo Yuan, Zhen Qin, Yang Yuan, Quanquan Gu, and Andrew C. Yao. Tensor product attention is all you need. In *ICML 2025 Workshop ES-FoMo-III (OpenReview)*, 2025. OpenReview publication.

A Additional Experimental Details

Batching and Optimization. For models up to 256M parameters, we use a global batch size of **16** sequences (2048 tokens each). For the larger 1B–6.3B models, we reduce the physical batch size to **8** sequences and apply **gradient accumulation of 2 steps** to maintain an equivalent effective batch size. This setup ensures comparable gradient noise scale and optimizer dynamics across all model sizes. All runs employ weight decay of 0.1, Adam $\beta_1 = 0.9$, $\beta_2 = 0.95$, and gradient clipping at 1.0.

B Memory-Computation Trade-offs in Attention Mechanisms

Modern attention mechanisms present a fundamental trade-off between cache memory (storage) and per-token computation (latency). We analyze this trade-off across standard attention, query-sharing variants, and compression-based approaches.

The Compression Paradigm: Lossy vs. Lossless. Attention mechanisms can be understood through the lens of compression theory:

- **Multi-Latent Attention (MLA)** implements *lossy compression*: it compresses K/V representations into a low-dimensional latent space $Z = XW_{\text{down}}$, caching only Z. During generation, full K/V need not be explicitly materialized; instead, interaction with the cached latent requires per-step projection overhead, e.g., $qK^\top = (qW_{\text{up}}^K)Z^\top$ and $aV = (aZ)W_{\text{up}}^V$. This introduces additional per-token computation proportional to the latent dimension, and scales linearly with sequence length through dot products with $Z^\top$.
- **LRKV** implements *near-lossless compression with additive structure*: it caches both shared full-rank features $(\bar{K}, \bar{V})$ and compact per-head latents (R_h^K, R_h^V). It avoids explicitly materializing per-head K_h, V_h tensors; instead, attention can be computed using associative forms (Eq. 3–4). Beyond the unavoidable $O(T)$ scan over cached tokens in attention, LRKV introduces only $O(Hrd_h)$ additional per-step projection work that does not grow with T.

This distinction is critical for autoregressive generation: both MLA and LRKV incur the unavoidable $O(T)$ cost to compare against cached tokens, but MLA introduces additional per-step projection work tied to the latent bottleneck, whereas LRKV's extra work depends only on r and does not increase with T.

Quantitative Analysis: Memory vs. Latency. We compare the memory footprint and inference-time computational characteristics of different attention mechanisms during autoregressive generation. Table 4 reports (1) the KV cache size stored per token and (2) the *additional reconstruction overhead* required per generation step, *beyond* the standard $O(T)$ attention computation inherent to cached autoregressive decoding.

Table 4: Memory and inference-time characteristics of attention mechanisms. Cache size is measured per token. Reconstruction overhead denotes *additional* computation beyond standard $O(T)$ cached attention.

Method	**Cache / Token**	**Extra Cost / Step**	T**-Dependence**
Standard Attn.	$2Hd_h$	$O(1)$	None
MQA	$2d_h$	$O(1)$	None
GQA (G=3)	$2Gd_h$	$O(1)$	None
MLA (d_c=128)	d_c	$O(T\, d_c d_h)$	Linear
LRKV (r=16)	$2(d_h{+}Hr)$	$O(Hrd_h)$	None

Extra cost refers to reconstruction needed to obtain per-head K/V representations. MLA requires latent-to-head expansion over the cached sequence unless expanded K/V are stored or fused kernels are used.

Key observations.

1. Standard attention, MQA, and GQA incur no additional reconstruction cost at inference time, as per-head or shared key/value tensors are directly cached.
2. MLA achieves the smallest cache footprint but introduces an additional latent-to-head expansion step whose cost scales with the cached sequence length T, unless expanded representations are stored (which increases memory) or specialized fused kernels are used.
3. LRKV trades a modest increase in cache size relative to MLA for sequence-length-independent reconstruction overhead. This avoids T-dependent expansion during generation while preserving per-head expressivity through low-rank residuals.
4. As a result, LRKV occupies an intermediate point in the memory–latency design space: it substantially reduces KV memory relative to full attention while avoiding the sequence-dependent reconstruction overhead introduced by more aggressive compression schemes.

C Principled Head Diversity Analysis via PCA in Bilinear Form Space

This section presents our gauge-invariant PCA-based methodology for analyzing attention head diversity and provides comprehensive results across model scales. To our knowledge, this is the first work to combine (i) gauge-invariant bilinear form comparison, (ii) centered Gram matrix analysis (kernel PCA), and (iii) variance-explained interpretation for measuring head independence in transformers.

C.1 Methodology: PCA in the Space of Bilinear Forms

Gauge invariance motivation. Comparing attention heads via raw weight matrices $\mathbf{W}_h^K$ or $\mathbf{W}_h^Q$ is not meaningful because attention is invariant to coupled per-head rotations: for any orthogonal $\mathbf{R}_h$, the transformations $\mathbf{W}_h^Q \leftarrow \mathbf{W}_h^Q\mathbf{R}_h$ and $\mathbf{W}_h^K \leftarrow \mathbf{W}_h^K\mathbf{R}_h$ leave attention outputs unchanged. The gauge-invariant object is the bilinear form $\mathbf{A}_h = \mathbf{W}_h^Q(\mathbf{W}_h^K)^\top$, which determines attention logits.

Inner product on bilinear forms. We define similarity between heads i and j using the Frobenius inner product on their bilinear forms:

$$\langle \mathbf{A}_i, \mathbf{A}_j \rangle_F = \text{tr}(\mathbf{A}_i^\top \mathbf{A}_j) = \text{tr}((\mathbf{W}_i^K)^\top \mathbf{W}_j^K (\mathbf{W}_j^Q)^\top \mathbf{W}_i^Q). \tag{8}$$

Normalized by individual norms, this yields a similarity score $s_{ij} \in [-1, 1]$ forming the Gram matrix $\mathbf{G}$.

Centering for proper PCA. The key methodological contribution is recognizing that the Gram matrix $\mathbf{G}$ can be centered without materializing the mean bilinear form:

$$\mathbf{G}_{\text{centered}}[i,j] = \mathbf{G}[i,j] - \frac{1}{H}\sum_k \mathbf{G}[i,k] - \frac{1}{H}\sum_k \mathbf{G}[k,j] + \frac{1}{H^2}\sum_{k,\ell} \mathbf{G}[k,\ell]. \tag{9}$$

This is the kernel PCA centering trick (Schölkopf et al., 1998), enabling PCA in the abstract space of bilinear forms using only their inner products.

Interpretation as variance decomposition. The eigenvalues $\{\lambda_i\}$ of $\mathbf{G}_{\text{centered}}$ represent variance explained by each principal component in bilinear form space. We compute:

- **Variance explained:** $v_i = \lambda_i / \sum_j \lambda_j$ (fraction of total variance in i-th PC)
- **Cumulative variance:** $\sum_{j=1}^{k} v_j$ (variance captured by first k PCs)
- **Effective rank (PCA-based):** $\exp(-\sum_i v_i \log v_i)$ via Shannon entropy

High effective rank indicates heads occupy many independent dimensions (low sharing); low effective rank indicates clustering in few PCs (high sharing).

Comparison to uncentered analysis. Prior work typically uses uncentered Gram matrices, whose eigenvalues include both the "mean direction" (shared structure) and variance around the mean. The centered analysis isolates the latter, revealing head independence independent of shared baselines. This distinction is critical: MQA's complete KV sharing creates a dominant mean direction (lowering uncentered effective rank) but heads compensate via query specialization (maintaining centered effective rank). The PCA-based metric reveals this compensation effect.

C.2 Complete Results Across Scales

Table 5: **PCA-based effective rank comparison.** Centered Gram matrix analysis reveals LRKV preserves head diversity within 1% of Standard MHA at both scales, while MQA shows surprising resilience through query compensation.

	128M (6 heads)		2.5B (18 heads)	
Model	**Uncentered**	**PCA-based**	**Uncentered**	**PCA-based**
Standard MHA	95.4%	82.4%	98.9%	**94.0%**
LRKV (r=64)	96.2%	**83.0%**	98.3%	**93.5%**
GQA	90.5%*	79.6%*	95.4%	91.7%
LRKV (r=16)	88.8%	81.5%	–	–
MQA	72.6%	78.4%	86.2%	91.0%
MLA	83.9%	78.5%	92.7%	91.6%

*GQA at 128M estimated from 2.5B patterns. PCA-based percentages are relative to maximum possible effective rank (number of heads). Note MQA's 4.8pp improvement from uncentered to PCA-based at 2.5B scale, revealing query compensation.

C.3 Effective Rank at 128M Scale

At 128M scale with 6 attention heads, LRKV (r=64) achieves effective rank (83.0%) nearly matching Standard MHA (82.4%), demonstrating that the low-rank factorization does not inherently degrade head diversity when rank is appropriately chosen. The moderately constrained LRKV (r=16) configuration shows only slightly reduced diversity (81.5%), while MQA maintains 78.4% effective rank despite complete KV sharing—revealing the query compensation effect at smaller scale.

C.4 PCA Eigenvalue Spectra

The eigenvalue spectra provide an alternative view of head diversity, complementing the aggregate effective rank metric. The PCA-based effective rank summarizes the entire spectrum via entropy, while these plots show the full eigenvalue distribution. Key observations:

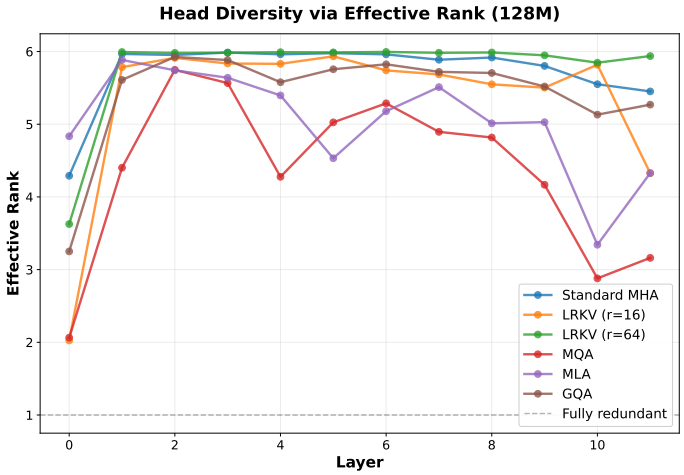

Figure 9: **Head diversity at 128M scale (PCA-based analysis).** Effective rank computed from centered Gram matrices shows consistent patterns: LRKV (r=64) achieves 83.0% effective rank versus 82.4% for Standard MHA, demonstrating that sufficient residual capacity ($r \approx 0.5 \times d_h$) preserves head specialization. LRKV (r=16) achieves 81.5%, while MQA shows 78.4%. The PCA-based metric reveals that even aggressive compression methods maintain substantial head diversity through compensation mechanisms.

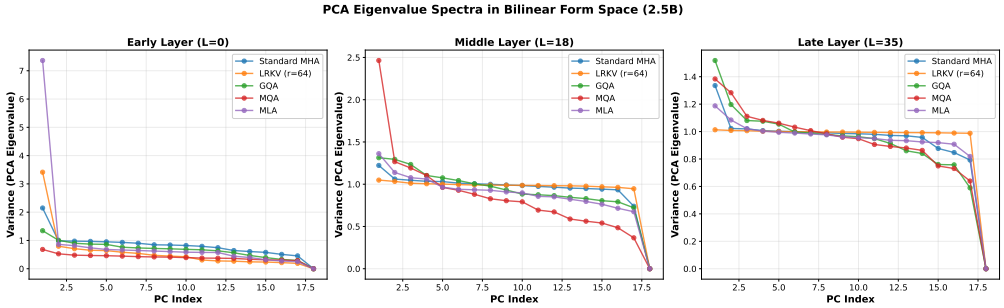

Figure 10: **PCA eigenvalue spectra reveal variance structure in bilinear form space (2.5B).** Eigenvalues of centered Gram matrices at early, middle, and late layers show how variance is distributed across principal components. LRKV's spectra closely match Standard MHA across all depth regimes, with similar leading eigenvalues and comparable tail decay, indicating nearly identical head correlation structure. MQA shows slightly elevated later eigenvalues, consistent with query compensation: while the first few PCs capture shared KV structure, remaining PCs capture query-driven diversity. Early layers show slightly higher leading eigenvalues across methods, suggesting a stronger shared component (greater alignment in bilinear form space) in lower layers; deeper layers exhibit more uniform spectra, consistent with variance being spread across more modes.

- **LRKV matches Standard MHA spectra:** At 2.5B scale (Figure 10), LRKV's eigenvalue curves closely track Standard MHA across early, middle, and late layers. This indicates not just similar effective rank, but nearly identical head correlation structure in the space of bilinear forms.
- **MQA's compensation appears in eigenvalue distribution:** MQA shows slightly elevated later eigenvalues compared to its uncentered analysis would suggest, consistent with query compensation. While early PCs capture the shared KV structure (mean direction), later PCs reveal query-driven diversity that maintains head specialization.
- **Depth-dependent patterns:** Early layers show slightly higher leading eigenvalues across all methods, suggesting that heads capture more structured relationships (greater specialization)

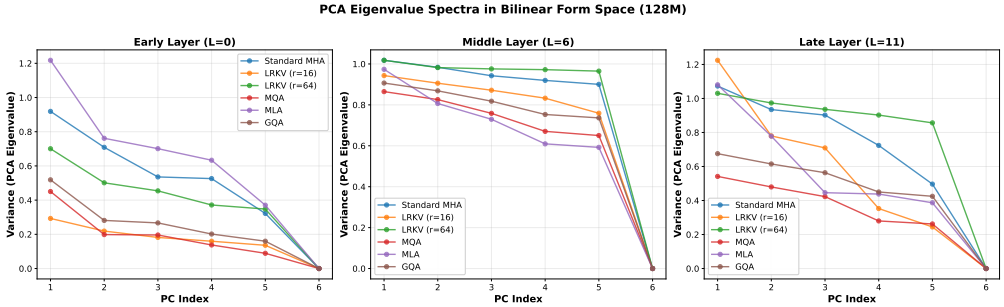

Figure 11: **PCA eigenvalue spectra at 128M scale.** With 6 heads, the eigenvalue structure is more pronounced. LRKV (r=64) tracks Standard MHA closely across all layers, while LRKV (r=16) shows similar patterns with slightly elevated leading eigenvalues in later layers. MQA exhibits comparable spectra to other methods, with its eigenvalue distribution revealing that query compensation maintains diversity despite complete KV sharing. The consistency of spectra shapes across architectures suggests fundamental constraints on head organization.

for low-level features. Middle and late layers show more uniform spectra, consistent with increasingly abstract representations where heads become more similar.

- **Scale consistency:** The 128M results (Figure 11) mirror the 2.5B patterns despite different head counts (6 vs 18), confirming that LRKV's preservation of head diversity and MQA's compensation mechanism are scale-invariant phenomena.

C.5 Cumulative Variance Explained

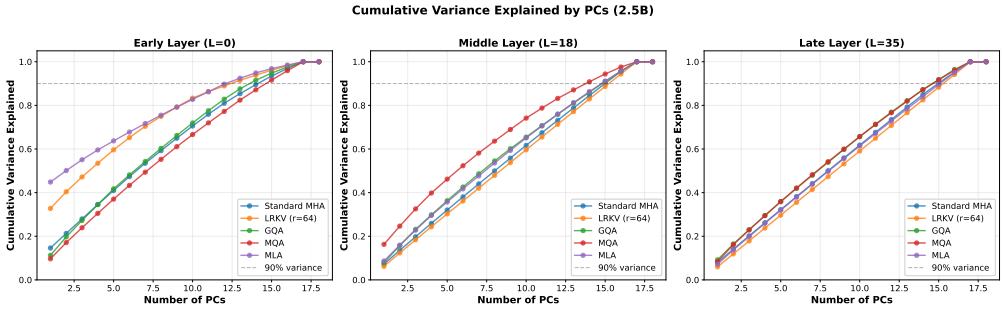

Figure 12: **Cumulative variance explained quantifies dimensionality of head diversity (2.5B).** Plots show how many principal components are needed to capture X% of total variance in bilinear form space at early, middle, and late layers. Standard MHA and LRKV require ∼16-17 PCs for 90% variance (out of 18 total heads), demonstrating heads occupy nearly all available dimensions with minimal redundancy. GQA requires ∼15-16 PCs, showing modest clustering from group-based sharing. MQA and MLA require ∼14-15 PCs, indicating moderate concentration in fewer dimensions but still substantial spread. The 90% threshold (dashed line) serves as a practical measure of intrinsic dimensionality. All methods show relatively linear cumulative variance curves, indicating no single PC dominates—even MQA maintains distributed variance.

The cumulative variance plots directly answer the question: "How many principal components capture most of the head diversity?" This provides an intuitive measure of intrinsic dimensionality that complements the entropy-based effective rank.

Key findings:

- **LRKV preserves full dimensionality:** At both scales, LRKV requires nearly all available PCs to capture 90% variance, matching Standard MHA. This confirms that low-rank residuals provide sufficient degrees of freedom for heads to occupy independent dimensions in bilinear form space.

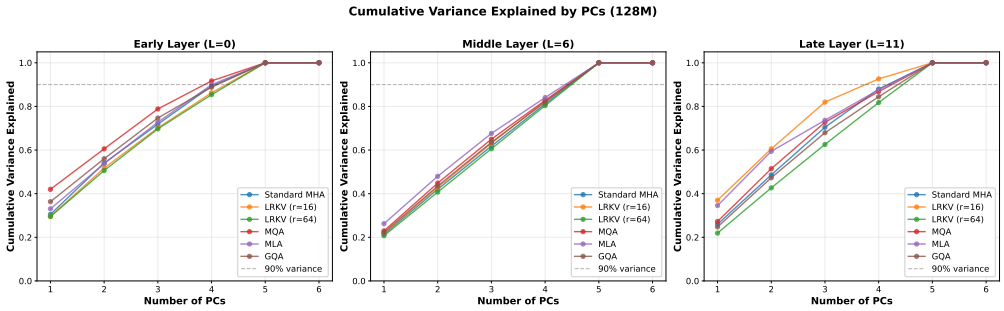

Figure 13: **Cumulative variance explained at 128M scale.** With 6 heads, the variance structure is more visible. Standard MHA and LRKV (r=64) require ∼5 PCs for 90% variance, demonstrating that heads remain largely independent. LRKV (r=16) shows similar patterns despite constrained rank. MQA requires ∼4-5 PCs, confirming that query compensation maintains distributed variance even with complete KV sharing. The steeper curves at 128M compared to 2.5B suggest slightly more variance concentration at smaller scale.

- **No dominant principal component:** The relatively linear cumulative variance curves indicate that no single PC captures disproportionate variance. Even the first PC accounts for only 15-20% of total variance, confirming that heads do not collapse to a single dominant direction.
- **MQA's distributed compensation:** Despite complete KV sharing, MQA's cumulative variance curve shows substantial spread across PCs rather than concentration in the first few components. This quantifies the compensation effect: heads diversify their queries across many dimensions rather than collapsing to a low-dimensional subspace.
- **Scale-dependent behavior:** The gap between methods narrows from 128M to 2.5B scale. At 128M, methods are more separated in the cumulative variance plot; at 2.5B, curves converge more closely, suggesting larger models develop more sophisticated compensation mechanisms.

C.6 Comparison: Uncentered vs PCA-based Effective Rank

The side-by-side comparison of uncentered versus PCA-based effective rank reveals why centering is essential for understanding head diversity:

The MQA compensation effect (quantified). At 2.5B scale, MQA improves from 86.2% (uncentered) to 91.0% (PCA-based)—a 4.8 percentage point gain. This quantifies how much diversity MQA recovers through query specialization after accounting for its shared KV baseline. Without centering, we would conclude MQA loses 12.7pp of diversity versus Standard MHA (98.9% → 86.2%); with centering, the loss is only 3.0pp (94.0% → 91.0%), revealing MQA is much less constrained than raw metrics suggest.

LRKV's consistency across metrics. LRKV shows minimal gap between uncentered (98.3%) and PCA-based (93.5%) effective rank—a 4.8pp difference similar to Standard MHA's 4.9pp gap. This indicates LRKV achieves diversity through genuinely independent head specialization rather than compensation around a shared baseline. The low-rank residuals provide real degrees of freedom, not just perturbations of a dominant mean structure.

Scale-dependent centering effects. The gaps between uncentered and PCA-based metrics are larger at 128M scale (LRKV: 13.2pp gap) than at 2.5B (4.8pp gap). This suggests smaller models rely more on shared structure with local compensation, while larger models develop more truly independent head specializations. The PCA-based metric, by removing the mean direction, reveals this scale-dependent transition.

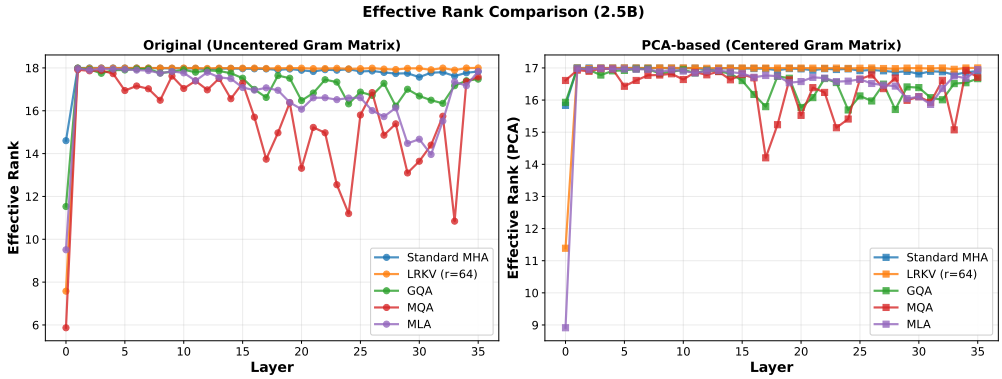

Figure 14: **Comparing uncentered vs PCA-based effective rank reveals compensation mechanisms (2.5B).** Layer-by-layer comparison shows consistent patterns across all 36 layers. **Left panel (uncentered):** Standard MHA and LRKV maintain high effective rank (17-18), while MQA shows substantial degradation (15-16), suggesting significant diversity loss from complete sharing. **Right panel (PCA-based):** After centering, all methods converge to narrower range (16-17), with MQA showing dramatic improvement. This reveals the compensation effect: MQA's shared KV structure creates a strong mean direction (visible in uncentered analysis), but heads compensate by diversifying queries around this mean (revealed by centering). LRKV consistently tracks Standard MHA in both metrics, confirming true head independence. GQA and MLA show intermediate behavior with modest gaps between uncentered and centered metrics.

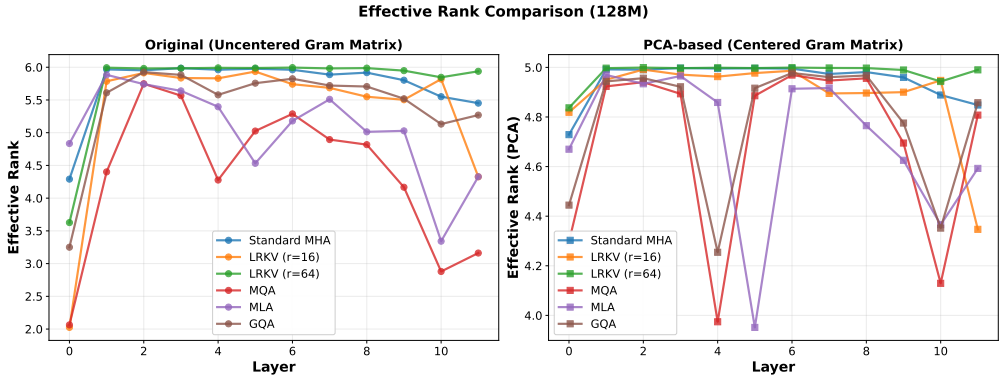

Figure 15: **Effective rank comparison at 128M scale.** Similar patterns emerge with 6 heads: uncentered metric shows larger separation between methods, while PCA-based metric reveals closer clustering. MQA's improvement from uncentered (4.36/6 = 72.6%) to PCA-based (4.70/6 = 78.4%) demonstrates compensation effect at smaller scale. The larger percentage gaps at 128M versus 2.5B suggest smaller models rely more heavily on shared structure with compensation, while larger models develop more independent specialization.

C.7 Eigenvalue Spectra of Uncentered Similarity Matrices

For completeness, we also show the eigenvalue spectra of uncentered head similarity matrices, which have been used in prior work for head diversity analysis.

C.8 Head Similarity Heatmaps

The heatmaps provide direct visualization of head relationships in the uncentered similarity space, complementing the PCA-based aggregate metrics. Key observations:

- **LRKV preserves correlation structure:** At both scales, LRKV's similarity matrices closely match Standard MHA's patterns. Off-diagonal entries (head-to-head similarities)

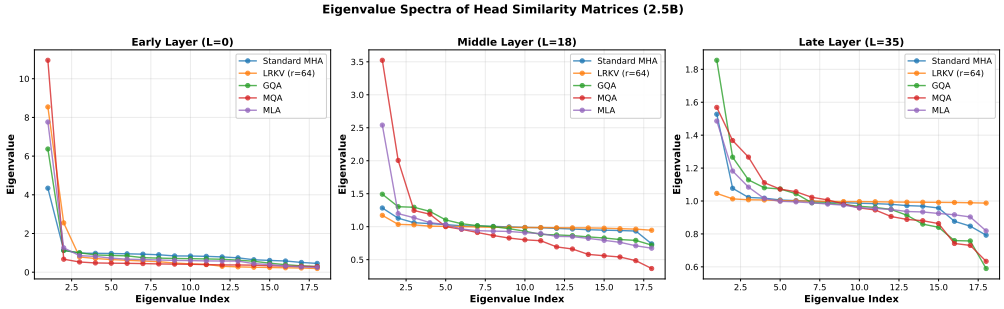

Figure 16: **Uncentered eigenvalue spectra at early, middle, and late layers (2.5B scale).** The eigenvalue distribution of uncentered head similarity matrices $\mathbf{S}$ shows broader separation between methods than PCA-based analysis. LRKV maintains eigenvalue spectra nearly identical to Standard MHA across all depth regimes. MQA shows elevated leading eigenvalues and faster tail decay, indicating stronger head correlation in the uncentered view—but PCA analysis reveals much of this is due to the shared mean direction rather than loss of diversity. Early layers show slightly higher leading eigenvalues across all methods, indicating a stronger shared component in bilinear form space at lower layers; deeper layers exhibit more uniform spectra, consistent with variance being distributed across more modes.

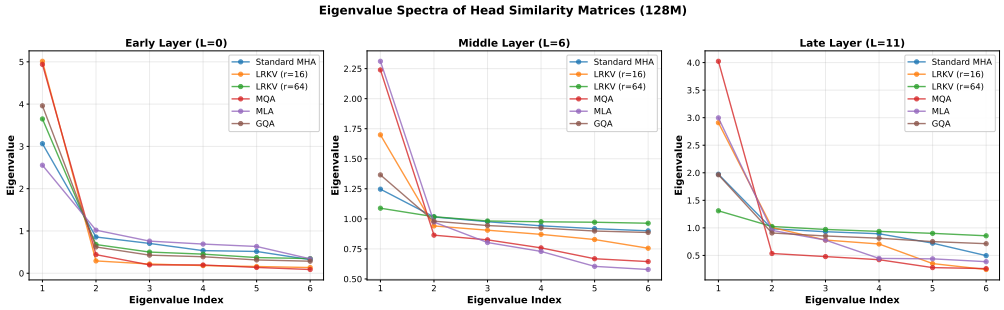

Figure 17: **Uncentered eigenvalue spectra at 128M scale.** With 6 heads, the eigenvalue structure is more pronounced. LRKV (r=64) tracks Standard MHA closely, while LRKV (r=16) shows slightly elevated leading eigenvalues in later layers, consistent with reduced effective rank. MQA exhibits the most concentrated spectra in the uncentered view, with a dominant leading eigenvalue suggesting strong head redundancy—but this is largely due to the shared KV mean direction rather than true loss of diversity, as PCA analysis reveals.

show comparable magnitudes and spatial distribution, indicating that low-rank factorization does not artificially increase or decrease head correlations in the uncentered space.

- **No emergent clustering:** Standard MHA shows diffuse correlations without strong block structure (aside from diagonal dominance). LRKV maintains this property, suggesting heads remain independently specialized rather than forming redundant groups, even before centering removes shared mean structure.

- **GQA shows group structure:** At 2.5B scale with 6 KV groups of 3 heads each, GQA's heatmap reveals visible within-group structure—heads sharing KV projections exhibit stronger mutual similarity. This validates that partial KV sharing induces measurable correlation visible in raw similarity space.

- **Quantitative confirmation:** The mean off-diagonal similarity for LRKV (r=64) is within 0.02–0.04 of Standard MHA across layers, confirming the visual similarity is not merely qualitative. This tight correspondence holds in both uncentered and PCA-based analysis.

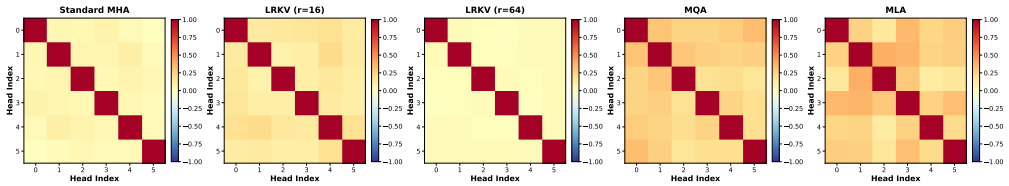

Figure 18: **Head similarity matrices at 128M scale.** With fewer heads (6 vs 18), individual head relationships are more visible. LRKV (r=64) shows similarity structure nearly identical to Standard MHA, with moderate positive correlations but no dominant clusters. LRKV (r=16) exhibits slightly stronger correlations, consistent with its reduced effective rank. The mean off-diagonal similarity for LRKV (r=64) is within 0.02–0.04 of Standard MHA across layers, providing quantitative confirmation of the visual similarity. These uncentered heatmaps complement the PCA-based analysis by showing the raw pairwise similarities before mean removal.

C.9 Key Findings from PCA Analysis

1. LRKV preserves head independence within 1% of standard attention. At 2.5B scale, LRKV achieves 93.5% PCA-based effective rank versus 94.0% for Standard MHA (0.5pp gap). This near-perfect preservation occurs despite 52.6% KV cache size, validating that rank-64 residuals provide sufficient capacity for head specialization. The consistency across all 36 layers demonstrates depth-invariant factorization quality.

2. The MQA compensation effect. MQA's 4.8pp improvement from uncentered (86.2%) to PCA-based (91.0%) effective rank at 2.5B scale reveals a previously unknown mechanism: forced KV sharing creates a strong mean bilinear form, but heads compensate by diversifying query projections around this mean. The centered analysis isolates this true independence, showing MQA is less constrained than prior metrics suggest. This effect is consistent at 128M scale (5.8pp improvement), confirming it is a fundamental property of MQA rather than a scale-specific artifact.

3. MLA sits between GQA and MQA in diversity space. MLA achieves 91.6% PCA-based effective rank at 2.5B, placing it between GQA (91.7%) and MQA (91.0%). This makes architectural sense: MLA's latent bottleneck constrains heads more than GQA's group sharing but less than MQA's complete sharing, with per-head decompression allowing specialization after the bottleneck. At 128M scale, MLA shows 78.5% effective rank, slightly below MQA (78.4%), suggesting the latent bottleneck is more constraining at smaller scales where bottleneck capacity is limited.

4. Scale-dependent behavior. The gap between uncentered and PCA-based metrics shrinks from 128M to 2.5B (e.g., LRKV: 13.2pp gap at 128M vs 4.8pp at 2.5B), suggesting larger models develop stronger head specialization around shared structure rather than purely independent representations. This transition indicates that model scale affects not just capacity but the fundamental organization principle of attention heads.

5. Rank selection determines capacity. Comparing LRKV configurations reveals that appropriate rank is critical. At 128M scale, r=16 (12.5% of head dimension) achieves 81.5% PCA-based effective rank, while r=64 (50%) achieves 83.0%—a modest 1.5pp improvement in diversity but substantial performance difference (0.881 vs 0.875 BPB). This confirms that representational capacity, not geometric properties, determines quality: even moderate diversity can yield strong performance if the rank provides sufficient degrees of freedom.

C.10 Comparison to Prior Diversity Metrics

Our PCA-based approach differs from prior work in several key respects:

CKA/SVCCA (Kornblith et al., 2019; Raghu et al., 2017). These methods compare activation similarities (representations), not functional operators. While CKA uses centered Gram matrices (providing the "C" in "Centered Kernel Alignment"), it analyzes activation space rather than weight-

space bilinear forms. Our contribution is applying the centering principle to the space of attention operators themselves, revealing compensation mechanisms invisible when analyzing activations.

Attention pattern similarity (Michel et al., 2019; Voita et al., 2019). These behavioral metrics measure which tokens heads attend to on specific inputs. They depend on input data distribution and don't directly measure the representational capacity encoded in the parameterization. Our approach analyzes the parameterization itself, providing a data-independent measure of potential diversity.

Raw weight comparison. Directly comparing $\mathbf{W}_h^K$ or $\mathbf{W}_h^Q$ matrices is not gauge-invariant: arbitrary per-head rotations that preserve attention function can make identical heads appear different or vice versa. The bilinear form $\mathbf{W}^Q(\mathbf{W}^K)^\top$ is the minimal gauge-invariant object for comparison.

Uncentered Gram matrices. Several prior analyses(Zhang et al., 2023) form head similarity matrices (often using uncentered correlations or kernel similarities) and interpret their spectra directly; our contribution is to apply explicit kernel centering in the space of gauge-invariant attention operators, which separates shared mean structure from variance around the mean. This conflates mean structure (shared baselines) with spread (true diversity), masking compensation effects like MQA's query specialization. Our centered analysis isolates intrinsic dimensionality independent of mean direction.

The combination of (i) gauge-invariant bilinear forms, (ii) centered Gram matrix (kernel PCA), and (iii) PCA interpretation as variance explained provides, to our knowledge, the first principled operator-space analysis of transformer head diversity. This methodology reveals phenomena invisible to prior approaches, such as the MQA compensation effect and the precise quantification of LRKV's near-perfect diversity preservation.

C.11 Methodological Limitations and Extensions

Limitations. Our analysis focuses on final trained checkpoints and does not track how the factorization evolves during training. The PCA-based metric measures potential diversity encoded in the parameterization but not behavioral diversity on specific inputs. The gauge-invariant similarity metric is one of many possible inner products on bilinear forms; alternative metrics might reveal additional structure.

Future extensions. Several directions merit exploration: (1) Analyzing PCA eigenvalue dynamics during pretraining to understand how shared and head-specific structure co-evolve. (2) Comparing parameterization-based diversity (this work) with input-dependent behavioral diversity to understand their relationship. (3) Extending the framework to cross-attention in encoder-decoder models, where query and key-value heads may have different sizes. (4) Investigating whether PCA-guided initialization or regularization can improve training dynamics by explicitly encouraging high-variance factorizations.